# Journal Pre-proof


CFD simulation of the BS 8414 test for Cladding Applications

Zhaozhi Wang, Fuchen Jia, Edwin R. Galea, John Ewer

PII: S0379-7112(25)00030-X

DOI: https://doi.org/10.1016/j.firesaf.2025.104366

Reference: FISJ 104366

To appear in: *Fire Safety Journal*

Received Date: 31 December 2023

Revised Date: 22 January 2025

Accepted Date: 21 February 2025

Please cite this article as: Z. Wang, F. Jia, E.R Galea, J. Ewer, CFD simulation of the BS 8414 test for Cladding Applications, *Fire Safety Journal*, https://doi.org/10.1016/j.firesaf.2025.104366.

# CFD simulation of the BS 8414 test for Cladding Applications

Zhaozhi Wang, Fuchen Jia, Edwin R Galea*, John Ewer,

*Corresponding Author: e.r.galea@gre.ac.uk

***Fire Safety Engineering Group, Centre for Safety, Resilience and Protective Security,***

***University of Greenwich, Old Royal Naval College,***

***30 Park Row, Greenwich, LONDON SE10 9LS, UK***



Highlights:

- A CFD fire model capable of simulating BS 8414 test has been developed
- The model is validated using data from BS 8414 tests of seven cladding systems
- Cladding cavity size is predicted to significantly impact fire spread
- Natural variations in wood crib HRR can compromise validity of BS 8414 results
- 30% mass reduction of PE core delays failure of BS 8414 test by only 60s

**Abstract**

A numerical BS 8414 model has been developed using surface ignition temperature, cone calorimeter data and a heat release rate curve from a wood crib, for simulating cladding fires. The model predicts burning rates of combustible materials, temperature profiles, burn-through of materials, burning locations and activation states of functional intumescent cavity barriers. The model is validated using seven DCLG BS 8414 tests, by correctly reproducing pass/fail results and failure mechanisms; producing comparable fire flames and reasonable agreement of temperature profiles, which are essential to the pass/fail criteria; and producing reasonable burning/burnt locations for the cladding system. The model has also been used to investigate factors affecting fire spread including cavity size, state of fire barriers, reduction of core

material mass by for example dripping and the consistency of the HRR behaviour of the wood crib fire source. The limitations of the BS 8414 model are discussed including the uncertainty of surface ignition temperature; the approach to the activation of intumescent cavity barriers; the uncertainties in HRRs of the wood crib fire and the material properties. To improve the repeatability of the BS 8414 test, it is suggested that a gas burner is used rather than a wood crib fire.

**Key words:** BS 8414 test, Wall cladding system, Fire spread, CFD numerical simulation.

## 1. Introduction

There have been many fire incidents involving combustible cladding materials resulting in human casualties, financial loss, and building damage. In 2010, a fire during installation of insulation material (polyurethane foam) occurred in a 28-storey residential building in Shanghai, causing 58 fatalities and 71 injuries [1]. In 2016, the fire of Address Downtown hotel in Dubai caused 15 injuries [2]. The 63-floor building was installed with Aluminium Composite Materials (ACM) panels with a flammable polyethylene core, which was blamed for the rapid fire spread both up and across the building. In 2017, 72 people lost their lives in the Grenfell Tower fire in London [3]. This 23-floor building, constructed in 1974 had a rainscreen cladding system, featuring ACM, installed as part of a renovation in 2015-2016. The fire in Grenfell Tower, which started on the 4th floor, spread rapidly both vertically and laterally with the ACM being identified as the main material contributing to the rapid external fire spread [3]. These rainscreen cladding system fire incidents have raised awareness and concerns, by the public and governments, regarding the use of combustible materials for external building walls.

After the Grenfell Tower fire, material requirements for the external walls of most buildings in England above 11 m have been updated in the 2020 and 2022 editions of Approved Document B (ADB) [4, 5]. There are two approaches identified to demonstrate compliance with the building regulations. One approach is to use bench-scale fire tests as recommended in the British standard BS EN 13501-1 [6], while an alternative approach is to use the larger scale 2017 BS 8414 fire test [7]. If the BS 8414 test results satisfy the criteria of BR 135 [8], the cladding system is deemed acceptable. There are a number of concerns with the 2017 BS 8414 test protocols [9] and several of these have been addressed in the recently (2020) updated test protocols [10] however, the current 2022 AD B still refers to the 2017 BS 8414. Most recently, the Grenfell Tower Fire Inquiry Phase 2 report [11] identified a number of concerns about the BS 8414 test protocols including, the lack of material thermal properties including ignition temperature, thermal inertia, heat of combustion, the lack of the rate of internal and external flame spread over the cladding system, the lack of data concerning toxicity of combustion products produced by burning cladding materials and the inadequacy of the simple pass/fail criteria.

There is also no scientific link between the BS 8414 test performance and how a building with a large quantity of the tested materials will perform in the event of a fire or the impact that such a fire would have on the occupants and occupant evacuation [11]. Further concerns about the BS 8414 test protocol [9] include not measuring the heat flux imposed on the façade; the fire load of the wood crib varying by at least a factor of two in different tests; the ventilation in the test facility is not adequately controlled and this may have a significant impact on the thermal attack on the façade systems being tested, etc. Furthermore, there are several practical issues that make routine BS 8414 testing challenging for many potential applications. Given the size and complexity of the BS 8414 test, there are limited facilities capable of performing the test.

Thus, demand for testing outstrips supply. This in turn impacts the cost of undertaking such a test.

The medium and large-scale fire tests [12-18] remain the only possible current routes to gain knowledge concerning the fire reaction of exterior facades. However, these assessments are financially expensive and time consuming. In contrast, numerical simulations based on Computational Fluid Dynamics (CFD) techniques are a cost-effective tool to investigate fire performance of cladding wall systems, including details such as the barriers and cavity size etc. There are several CFD software tools available capable of simulating the burning of solid combustibles, including Fire Dynamics Simulator (FDS) developed by NIST US [19], FireFOAM developed by FM Global, US [20], and SMARTFIRE developed by University of Greenwich, UK [21] etc. Yuen et al. published a comprehensive review [22] of wall cladding fires including related CFD simulations. Given the high computational cost associated with simulating large full building geometries and the complexity of cladding fires, most CFD simulations are restricted to investigating the impact of a fire on the exposed cladding, excluding the burning and mechanical failure of cladding materials or the spread of fire within the cavity formed between two parallel walls [23-25]. Anderson et al. [26] conducted a comparative simulation study on three large-scale facade testing methods, namely, the SP Fire 105, BS 8414-1, and the ISO 13785-2 methods. The HRRs in these simulations were based on experimental data or were approximated from the literature. Kotzen et al. [27] demonstrated the potential of SMARTFIRE for simulating BS 8414 fire tests, including living wall assemblies, excluding plants.

Hassan [28] developed a cladding fire model and validated it by simulating one BS 8414 fire test. The model applied a pyrolysis model with an ignition temperature of 380 $^{O}$C for the PE

core while the aluminium cover is removed from the simulation when its temperature reaches 600 $^{O}$C. Dréan et al. [29] developed a CFD model for cladding fire and validated it using medium-scale fire tests according to ISO13785-1 with ACM-PE-based cladding. In their CFD model, the ignition of the ACM panel was based on the ignition temperature of PE i.e., 380 $^{O}$C, and a uniform fine mesh of 0.02 m was used throughout the solution domain. This model was also further validated by simulating one of the large-scale DCLG BS 8414 tests i.e., DCLG test 1 [14], using the same model parameters [30], producing good agreement with the test results. However, practical engineering CFD applications for high-rise buildings generally require a significantly coarser mesh resolution due to the computational expense associated with finer mesh resolution. Dréan et al. also simulated three of the DCLG BS 8414 tests i.e., DCLG tests 1, 2, and 5 using a coarser mesh size of 0.125 m for the combustion chamber and 0.25 m for the extended volume of the facility [30]. To be consistent with the use of the coarser mesh, the size of the cladding cavity in the simulations was increased from 0.055 m (as implemented in the fire tests) to 0.25 m for the coarse mesh simulations. Furthermore, for this coarse mesh to produce reasonable agreement with the measured experimental data and observed experimental trends, the ignition temperatures for each material were artificially modified, requiring them to be decreased by 100 $^{O}$C, i.e., for PE the ignition temperature was changed to 280 $^{O}$C. In a further numerical study by Dréan et al., the influence of wind and fire source on the BS 8414 test was investigated with a mesh size of 0.05 m [31]. In a later study, again using the coarser mesh size of 0.25 m and the artificially reduced ignition temperatures, the model by Guillaume et al. produced reasonable agreement with the observed pattern of burning for the vertical cladding fire on the east face of Grenfell Tower [32]. Furthermore, Guillaume et al. simulated the fire spread over the entire exterior of the Grenfell Tower [33]. By ignoring the impact of wind, it was possible to simulate the entire exterior of Grenfell Tower fire using separate simulations of the east wall, north wall, west wall and south wall fires. The investigation

exploited the symmetry of the building to reduce computational effort, by constructing only two geometry models, i.e., the east (or west) wall and north (or south) wall.

In theory, the criterion of surface ignition temperature alone is sufficient for the simulation of fire spread along combustible solid surfaces. However, as pointed by Jia et al. [34, 35], the sole use of surface ignition temperature as the ignition criterion, can make the prediction of fire spread strongly mesh dependent if there is a small ignition source. As fire is a complicated and multi-scale phenomenon, it would be extremely difficult, if not impossible, to eliminate this reliance altogether from simulations of fire spread over solid surfaces. Therefore, as a practical engineering method, parameters such as the critical incident heat flux or flame spread rate are introduced, alongside surface ignition temperature, in enhanced flame spread models used in fire simulations [36- 40].

The aim of this study is to develop a computer model capable of reproducing the BS 8414 test. The primary purpose of the BS 8414 model is to reduce the cost associated with BS 8414 testing by providing a means to pre-test cladding systems, thereby reducing the number of cladding systems that need to undergo a physical BS 8414 test. Only products that clearly pass the numerical test would need to be fully tested. Furthermore, the computer model can be used to identify reasons for cladding failure and investigate cladding fire characteristics. Compared with the other models and studies addressing cladding fires [28- 33], the model presented here consists of four additional features. Firstly, the mesh size is limited to 0.0125 m within the cavity, 0.03 m in the external region near the cladding and 0.17 m at remote locations. This non-uniform mesh takes into consideration the mesh requirements for capturing the combustion phenomenon (as suggested by Dréan et al. [30]) while reducing computational costs compared to a uniform fine mesh. The non-uniform mesh provides sufficient flexibility

to accurately represent the actual cavity dimensions and enable a reasonable representation of the cavity airflow, without using an excessively fine mesh for the whole computational domain (as in the fine mesh study in [30]) or an excessively coarse mesh which does not accurately represent the cavity thickness (as in the course mesh studies [30] and [32,33]). Secondly, rather using the ignition temperature of the core material as a criterion for the ACM panel, a more physically appropriate ignition temperature of 550 $^{O}$C is used which relates to the covering Aluminium sheet. This is based on the properties of the Aluminium of the integrated ACM panel that takes into consideration the protection against ignition offered to the core material by the aluminium covering sheets. Thirdly, to reflect the different burning characteristics of the unprotected edges of the ACM panels, a second ignition criterion is used with a lower ignition temperature than that used for the surface panel. Fourthly, in addition to ACM materials with PE core, cladding fire tests involving FR PE are simulated in this study. The fire simulation software SMARTFIRE [21] is used in this study. The model is presented in Section 2. The developed model is validated by simulating the seven DCLG BS 8414 tests in [14] with the simulation set up as presented in Section 3, and the simulation results analysed in Section 4. The HRR from the burning of individual materials of the cladding system, the impacts of the cavity size; the cavity barrier and intumescent activation; and the reduction of the amount of polyethylene (PE), which is used in the core of some aluminium composite panels; the uncertainty of the wood crib fire source on the cladding fire spread and the impact of thermocouple location, are investigated in Section 5. The limitations of the developed BS 8414 Simulator are discussed in Section 6. Finally, the conclusions are drawn in Section 7.

## 2. The BS 8414 Simulation Model

A research version of SMARTFIRE V5.1 software [21] is the framework of the BS 8414 model. The CFD engine in SMARTFIRE has many physics features that are required for fire field modelling, that have been described previously many times in the literature [36-40], so their description is not repeated here. These sub-models include k-epsilon turbulence model; flame spread model; gaseous combustion model (eddy dissipation combustion model) [41]; smoke model, toxicity model, etc. It is worth noting that the radiative transfer equation (RTE) is solved using the discrete ordinates method (DOM) with 48 rays. The absorption coefficient, $a_m$, of the smoke contaminated air mixture is given under a gray gas assumption by $a_m = a_s + a_g$ where $a_s$ and $a_g$ are the absorption coefficients of soot and gases respectively. $a_s$ is proportional to the product of smoke volume fraction and temperature [21] and $a_g$ is a function of the concentrations of $CO_2$ and $H_2O$ and temperature [42].

The flame spread model is the core of the BS 8414 Simulator and is described in detail here. The flame spread model in SMARTFIRE was initially developed to simulate an aircraft fire [34]. In this model, all combustible surfaces are assigned a face patch type which identifies them as a burnable material. Each face patch is labelled with a unique patch number which defines their location and material properties. At the end of each time step, conditions at a cell face of a potentially burnable face patch are assessed to determine if ignition conditions are reached. The ignition of the material is determined by either of the following ignition criteria:

(a) The material surface temperature reaches the prescribed ignition temperature;
(b) The advancing pyrolysis front spreads from an adjacent burning cell face to the cell face being considered;

If one of these ignition criteria is reached, the cell face begins to burn. Once a cell face is ignited, it starts to release a certain amount of fuel according to the time dependent burning rate ($kg/m^2s$) or HRR for this material, for which data has been collected from small-scale tests.

In the work of Hu et.al. [35], the flame spread model was further modified to reduce its mesh dependence and has been used in a number of applications including forensic reconstructions of the Station nightclub fire [36], the Manchester Airport B737 fire [38] and a shooting range fire [40]; simulations of a rail car fire and an aircraft cabin fire [35, 43] and the fire safety assessments of a Blended Wing Body (BWB) aircraft cabin and wide wing open wide gangway underground trains [37, 39].

One important issue in modelling the BS 8414 testing of a cladding wall system with ACM is how to represent the thin composite material panels. In the DCLG BS 8414 tests [14], the ACM panel consists of a 0.003 m thick core material layer sandwiched between two 0.0005 m thick aluminium sheets. In this study, the thin ACM panel is represented by a dynamically controlled three-layer face patch. A 1-D heat conduction calculation is performed using the actual thickness of the three-layer ACM panel. For the BS 8414 Simulator, Criterion (a) is the dominant one once the fire is sufficiently large to sustain the fire development. The effect of criterion (b) is significant only in the very early stage of fire development when the fire is weak and the dominant heat transfer for flame spread is convective [35]. An ACM surface ignition temperature and flame spread rate is specially set for the burning of ACM in Section 3 later. Once the solid core material of the ACM panel at a specific face cell is burnt off, a burn-through of the ACM occurs, which is modelled by the removal of this solid face cell. The burnt off solid face cells further affect the integrity of the cavity.

Intumescent barriers in the cladding system are used to prevent both vertical and horizontal fire spread within the ventilation cavity. These barriers are activated when heated by the fire effluents and then expand to block the air gap between the internal insulation layer and the ACM panel. The expansion of the intumescent is modelled as an additional solid obstacle that fills the space between the surface of inactivated intumescent barrier and the ACM panel. This occurs cell-by-cell when the gas temperature in a cell between the barrier and the ACM panel

reaches a prescribed critical value, and after a prescribed delay to allow for activation of this cell.

The ignition source of the BS 8414 test, a wood crib fire, is a critical factor for the cladding fire to develop. SMARTFIRE has developed a specific wood crib fire model for the BS 8414 Simulator. The wood crib model is a porous volumetric source, with the same size of the wood crib used in the test, i.e., 1.0 × 1.5 × 1.0 m and with a porosity of 0.5 representing the solid to air occupation of the cribs in the entire wood crib volume. The volumetric fire source is calibrated to obtain a flame shape and temperature profiles at external level 1 and 2 that are as close as possible to the observations and temperature measurements in DCLG BS 8414 test 6 (consisting of limited combustibility mineral as ACM core and stone wool as insulation) [14] and an additional test in which a cladding wall system was absent.

The full set of model input parameters for the BS 8414 simulations are summarised as:

- Molecular structure of wood and ACM core respectively (for the different chemical reaction equations of the wood crib fire and cladding fire);
- Surface ignition temperature ($^{O}$C) of the ACM panel and the insulation;
- Thickness (m) of the cladding panels and insulation;
- Density (kg/m$^3$) of each material used in the cladding system;
- HRR per unit area (kW/m$^2$) (under various external irradiance levels) of ACM core and insulation materials;
- Specific heat (J/kg) of all materials;
- Thermal conductivity (W/mK) of all materials;
- Critical temperature ($^{O}$C) and the delay duration (s) for the intumescent to expand to fill the cavity width of the cladding system;

- Mass loss rate of the wood crib fire (kg/s);

The BS 8414 model is expected to be capable of:

- producing the measurements and fire behaviour observations consistent with the current requirements of the BS 8414 protocol including:
  - the temperature profiles, as a function of time, at individual locations;
  - the developing fire plume as a function of time;
  - the final state of damage of the cladding system including the burnt through regions of the ACM panel, etc.
  - a pass/fail result for the cladding system with the cause identified.
- providing additional quantification of relevant fire behaviour including;
  - the HRRs for each material component of the cladding system such as the ACM panel and the insulation.
  - the lateral and vertical flame spread rates of the cladding system.
  - the burning/burnt off locations of the ACM panel and insulation, as a function of time;
  - the activation state of barrier intumescent strips, as a function of time, and their representation as obstructions in the cavity, once activated;

With these additional capabilities, the modelling of the BS 8414 test provides further insight into important issues that are not currently explored in actual BS 8414 physical experimentation including:

- sensitivity of the developing fire behaviour to cavity size (see Section 5.2);
- sensitivity of the pass/fail outcome to the representation of the wood crib fire (see Section 5.4).
- potential mitigation measures to improve the fire safety performance of the proposed cladding system (see Section 5.6).

- the impact of cavity thermocouple location on the pass/fail outcome (see Section 5.7).
- sensitivity of material properties on the pass/fail outcome (see Section 6).

## 3. Simulation Setup

### 3.1 The computational geometry

Presented in Fig. 1 is an overview of BS 8414 [8] test facility and the layout of cladding panels in the DCLG BS 8414 tests [14]. The test facility represents the face of a building and consists of a masonry, or masonry infill, structure with a vertical main test apparatus wall and a vertical return wall (wing) at a 90° angle to, and at one side of the main test wall. The dimensions of the two walls can be seen in Fig. 1. The combustion chamber is positioned at the base of the main vertical test wall such that the fire flames will project through the opening at the base of the main vertical test wall. The crib within the combustion chamber is 1.5 m × 1.5 m in plan view and 1.0 m high, consisting of kiln-dried softwood sticks with a peak heat output of 3.0±0.5 MW and a total heat output of 4500 MJ over 30 minutes. In the test protocol, temperatures at two heights, Level 1 and Level 2 are measured using thermocouple arrays. Level 1 and Level 2 are located 2.5 m and 5.0 m above the top of the combustion chamber respectively. External air temperatures (0.05 m from the surface) are measured at both levels, while temperatures at the midpoint of the cavity and internal temperatures at the midpoint of the insulation layer are measured at Level 2.

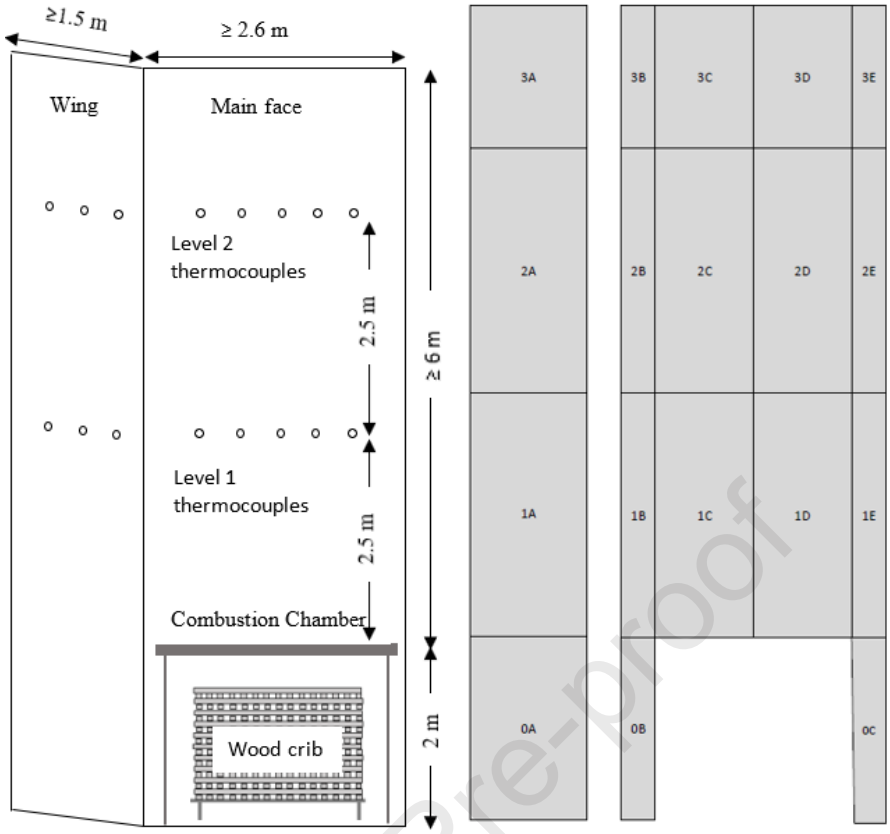


Fig. 1. Schematic of BS 8414 test facility (left) and layout of cladding panels in DCLG BS 8414 tests (right) [14].

The dimensions of the computational domain used to describe the BS 8414 test facility are 5.0 m × 11.0 m × 5.5 m with outlet patches for the open boundary at the sides and the top of this domain. The SMARTFIRE set up of this domain is shown in Fig. 2a.

Presented in Fig. 2b is a schematic of the cladding system with PE as the ACM core and with a 0.1 m thick layer of insulation attached to the outer wall surface. The setup in the model, of the structure of the test facility and the installed cladding system, is shown in Fig. 2c using the exact sizes of ACM panels, cavity and insulation according to the DCLG BS 8414 test reports [14]. The computational mesh used in the analysis is described in Section 3.4.

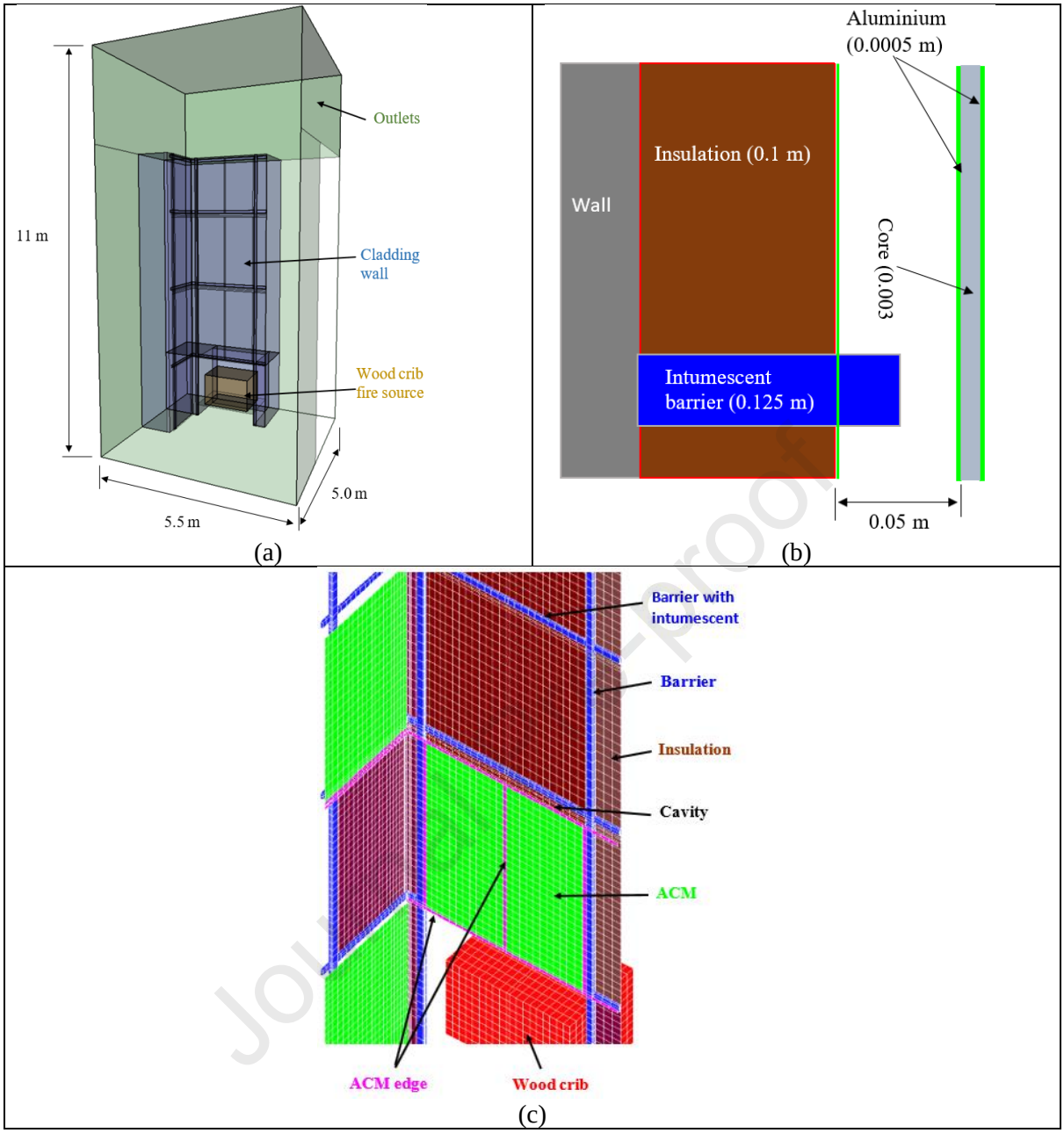


Fig. 2. (a) Computational domain of the BS 8414 Simulator; (b) schematic of the cladding system (insulation thickness varies with scenarios); (c) set up of ACM panels, insulation, barriers, and wood crib fire volume.

The external and cavity thermocouples are not physically modelled in the simulations. The simulated thermocouple temperature is simply the air temperature at a 0.04 m size cell. The centre of this cell is the location of a thermocouple which was installed in the fire test (see Fig. 1 and the test report [14] for thermocouple locations).

### 3.2 Wood crib heat release rate

Unfortunately, the HRRs for the wood crib fires used in the DCLG BS 8414 tests [14] described in this paper were not measured or reported. Furthermore, the British Standard for BS 8414 [8] allows for a wide range of wood crib peak HRRs ranging from 2.5 MW to 3.5 MW. Thus, the peak HRR in the DCLG tests could have varied between these peak values and could have been different in each of the seven fire tests. This provides for a wide range of possible HRR curves that could be used in the fire simulations presented in this study. For consistency, a single HRR curve was used for all seven DCLG BS 8414 fire tests. Furthermore, the HRR curve used in the simulations was based on the measured heat release rate curve derived for a BS 8414 test without cladding [44] (see Fig. 3). The HRR curve used in the simulations, while based on that from [44], was adjusted so that the predicted cladding performance was consistent with the measured results for the DCLG tests while producing a peak HRR of 2.5 MW (see Fig. 3).

It has been demonstrated that this peak HRR is capable of reproducing the observed fire flame height in a DCLG BS8414 test without an installed cladding system (see Supplementary Material Section S1).

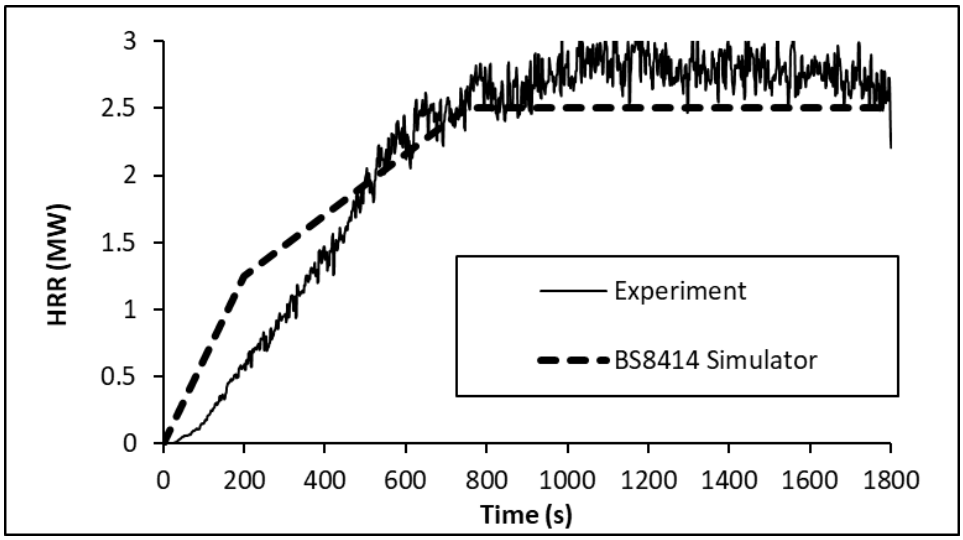


Fig. 3. HRR for the wood crib fire used in the BS 8414 Simulator.

### 3.3 Material properties

The dimensions of the various cladding system configurations examined in the seven DCLG BS 8414 tests [14] are presented in Table 1 and are used in the simulations. The material properties such as density, conductivity and specific heat, are presented in Table 2. As the material properties for the specific cladding systems used in the DCLG BS 8414 tests are not presented in the test report, as noted in Table 2, average data from the literature are used in the simulations. One challenge in cladding fire simulations is the lack of model parameter data for some building materials. Both the specific heat capacity and thermal conductivity for FR PE are unavailable from the literature. The impact of fire retardant components in the FR PE on fire development is complex including delaying the ignition time and reducing the peak HRR. Compared with the average ignition time of 84.9 s for ACM with PE core, the average ignition time for three investigated FR PE ACM is delayed by 18.4 s or 21.7% [45]. As a crude approximation for the material properties of FR PE, its density and thermal conductivity are assumed to be the same as for PE but with a high specific heat capacity value to represent the likely delay in ignition compared to PE. This high specific heat capacity value is estimated to be approximately 2300 J/kgK (derived by multiplying the adopted specific heat value of 1900 J/kgK for PE and the ignition time ratio of 121.7%). The specific heat capacity of phenolic and the limited combustibility material used in the DCLG fire tests are also unavailable. In the simulation of DCLG test 5 by Dréan et al., [30] the thermal properties of PE are used for the limited combustibility material, but the limited combustibility material is assumed incombustible. This assumption limits the burn through of the ACM panel, which impacts the combustion environment of the insulation. In this study, a medium specific heat capacity of 1200 J/kgK is assumed for the phenolic foam and a large value of 2300 J/kgK is assumed for the limited combustibility material. Given the uncertainties in some of the material properties,

sensitivity analysis was conducted to explore how simulation outcomes varied based on selected material property values (see Section 6).

Table 1 The thicknesses of the cladding system in the seven BS 8414 tests

| | **ACM** | | **Air gap** | **Inner Insulation Materials** | | |
|---|---|---|---|---|---|---|
| | **Aluminium** | **Core** | | **PIR** | **Stone wool** | **Phenolic** |
| **Thickness (m)** | 0.0005 | 0.003 | 0.05 | 0.1 | 0.18 | 0.1 |

Table 2 General material properties

| **Material** | **Density (kg/m$^3$)** | **Conductivity (W/mK)** | **Specific heat (J/kgK)** | **Note** |
|---|---|---|---|---|
| **Aluminium** | 2700 | 237 | 9007 | [21] |
| **Wood** | 800 | 0.17 | 2380 | [21] |
| **PE** | 925-950 [45] | 0.3-0.38 [46] | 1550 [46]<br>1650 [45]<br>1900-2300 [47] | Values of 925, 0.33 and 1900 are used in the simulator for the three material properties |
| **FR PE** | 970-1410 [48]<br>1265-1650 [45] | | | Values of 925, 0.33 and 2300 are used in the simulator for the three material properties |
| **PIR** | 30.4-31.2 [14] | 0.02-0.04 [48] | 1100 [29]<br>1257 [50]<br>1670 [46] | Values of 31.2, 0.02, 1100 are used in the simulator for the three material properties |
| **Stone wool** | 47.7 [14] | 0.03-0.05 [49] | 1000 [31] | Values of 47.7, 0.04, 1030 are used in the simulator for the three material properties. |
| **Phenolic** | 32.0 [14] | 0.029-0.041 [49]<br>0.015-0.11 [51] | | Values of 32, 0.02 and 1200 are used in the simulator for the three material properties |
| **limited combustibility material** | 1625 [45] | 0.033-0.045 [49] | | Values of 1625, 0.033 and 2300 are used in the simulator for the three material properties |

The combustion of an ACM panel and insulation materials that are covered with an extremely thin layer of aluminium foil, is complex. Exposed to heat, aluminium will expand, deform, and even melt. This results in the connection failure of the aluminium sheets or foil attached to the burnable materials. Therefore, if the ignition temperature of the core material of an ACM panel is lower than the melting point of aluminium (660 $^{O}$C), the ignition temperature of the ACM panel should be between the ignition temperature of the pure combustible core material and the melting point of aluminium. Furthermore, it is noted that aluminium completely loses its strength at 550 $^{O}$C in fire [52] and so is likely to be unable to protect the burnable material above this temperature. Therefore, instead of the surface ignition temperature of its core material, the surface ignition temperature of an ACM panel is assumed to be the maximum of 550 $^{O}$C and the surface ignition temperature for the burnable material.

At the edges of the ACM, the protection offered by the surface layer of aluminium to the core material is greatly reduced as the edge of the core is exposed. This is supported by evidence from images and observations of advancing flames along the gaps between panels in large scale tests [14] and evidence from cone calorimeter testing where the time until ignition of ACM panels with holes was reduced compared to the same panels without holes [53]. These observations support the introduction of a secondary ignition temperature for the exposed edges of ACM panel in cladding fire simulations.

Thus, it is assumed that the surface ignition temperature for the ACM edge is between the ignition temperature of its core and 550 $^{O}$C. For example, for the ACM panel with PE core, the edge ignition temperature is set to 480 $^{O}$C (Table 3). The edge surface ignition temperature of 480 $^{O}$C is calibrated from simulations for ACM with PE core, but is equally applicable for other ACM panels where the ignition temperature of the core material is less than 550 $^{O}$C. Due to

the observed ignition behaviour of ACM panels in fire tests, but without definitive quantification of the ignition temperature of aluminium protected core material at either the surface or edge of a cladding panel, it is a reasonable assumption for modelled behaviour to use the two different ignition temperature values for the edge and non-edge areas of a composite material with aluminium covers as suggested above. These ignition temperatures are between the pure fuel ignition temperature and structural deformation temperature of the aluminium.

It is noted that in tests 5 and 6, the ACM core was identified as a limited combustible material and so is likely to have an ignition temperature greater than 550$^{O}$C. However, using the ignition temperature values of 550$^{O}$C and 480$^{O}$C for the surface and edge ignition criteria, a preliminary simulation of DCLG test 5 (with limited combustibility material for the ACM core and a PIR insulation) suggests that the HRR contribution from the burning of the limited combustibility material is no more than 0.022 MW (see Supplementary Material Section S2, Fig. S7). This HRR contribution is less than 1% of the HRR of the wood crib fire source, which is much less than the accepted uncertainty for the wood crib HRR in the BS 8414 test protocol. Given that the HRR contribution from the limited combustibility material, while using the 550$^{O}$C and 480$^{O}$C for the surface and edge ignition criteria, is very small, it is unlikely to significantly impact the results. Therefore, using the specified surface and edge ignition criteria is applicable for ACMs with a limited combustibility material core.

It is also noted that an originally non-edge face cell will automatically become an edge cell once any of its neighbour cells has been burnt out. As a result, its surface ignition temperature of 550 $^{O}$C, correspondingly changes to 480 $^{O}$C.

The flame spread rate used in criterion (b) depends not only on the material properties of the surface, but also the nature of the fire scenario investigated. In the BS 8414 simulation model, a flame spread rate of 0.0001 m/s is used (estimated from BS 8414 tests with cladding materials of limited combustibility e.g., DCLG tests 5 and 6). This value is much less than the value used in previous fire simulations involving interior aircraft cabin panels (0.003 m/s) [38, 43], which consist of different materials to those tested in the DCLG tests. However, in the BS 8414 fire simulations, the fire development is generally dominated by the criterion of surface ignition temperature (i.e., criterion (a)) due to the large wood crib fire source.

Table 3 Combustion properties

| **Material** | **Ignition temperature ($^{O}$C)** | **Heat of combustion (MJ/kg))** | **Note** |
|---|---|---|---|
| **Wood** | 433 [35] | 17.8 [46] | For materials covered with aluminium, instead of the ignition temperature of the material, a surface ignition temperature of 550 $^{O}$C is applied.<br><br>The ignition temperature for a panel edge (irrespective of core material) is 480 $^{O}$C. |
| **PE** | 377 [46] | 41.4 [45] | |
| **FR PE** | 339-397 [54] | 23-25.1 [45] | |
| **PIR** | 378, 435 [46] | 19.2-21.6 [45] | |
| **Stone wool** | >1000 | 22.7 [45] | |
| **Phenolic** | 429 [3] | 20.2-23.7 [45] | |
| **limited combustibility mineral** | >1000 | 6.2 [45]<br>2.4 [14] | |

As reviewed by Hjohlman et al. [55], the heat flux measured in large-scale compartment fire experiments received by seating is around 35 kW/m$^2$ and for other furniture in the test compartment, the heat fluxes are around 50 kW/m$^2$. Therefore, the cone calorimeter HRR data for these materials, under corresponding heat fluxes, is likely to be a close representative of their burning behaviours in these test fires. Furthermore, the HRRs (or mass lost rate) obtained

from cone calorimeter experiments, under an irradiance level of 50 kW/m$^2$, have been used to simulate cladding wall fires [30-33] and enclosure spread fires [36-40, 43]. Thus, the HRRs obtained from cone calorimeter experiments, under an irradiance level of 50 kW/m$^2$, are used in the simulations presented in this study. It is acknowledged that in large-scale cladding fires, the external components of the cladding system may be subjected to higher irradiance values, and if this occurs sufficiently early in the fire development may have an impact on the speed of fire development (see the discussion in Section 6). The HRRs for each ACM core and insulation material can be found in [45]. The HRRs are commonly measured from 0.004 m thick test samples [45]. However, the ACM cores, in the DCLG BS 8414 tests, are only 0.003 m thick [14]. It is thus necessary to modify HRR data of the 0.004 m thick material to be representative of the 0.003 m thick material. This is achieved by ignoring volume/area and insulation differences of the sample and assuming a proportionate rate of heat release, thus finding a time to which the cumulative released heat is three quarters of the total released heat from the test with a 0.004 m thick material. The tail of the HRR curve, after this time, is truncated. The remaining part of the HRR curve is used in the simulation representing the HRR from a 0.003 m thick material (See Fig. 4 for example). The zero time of the HRR used in the simulation is when the HRR curve starts to rise rapidly. As shown in Fig. 4, once the material is ignited in the BS 8414 simulation, it will start to release heat from 110s (zero time in the simulation). The HRRs for other materials used in the current simulations (i.e., Phenolic, FR-PE, PIR, Mineral wool and limited combustibility material) are derived from McKenna et al. [45] and are presented in Supplementary Material Section S3, Fig. S8.

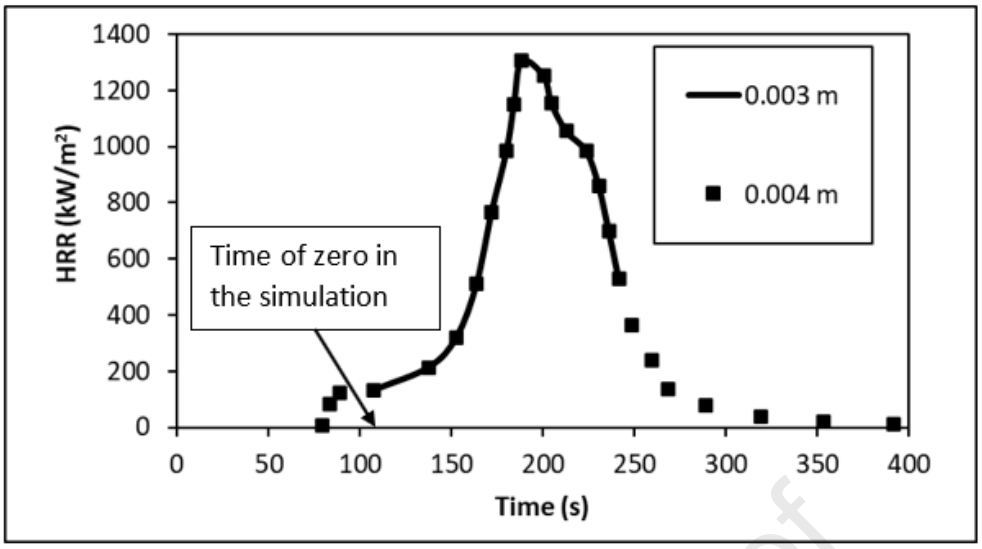


Fig. 4. Experimental HRR dada of 0.004 m PE and the HRR curve of 0.003 m PE used in the simulation.

The gaps around the edges of the installed panels in the experimental setup are complex, with the vertical and horizontal gaps being treated differently in the test installation. The horizontal gaps between upper and lower ACM panels are of the order of 0.02 m and create a flow path between the cavity and the outside. These gaps have been included in the model as actual gaps with exposed panel edges. The vertical gaps between the left and right ACM panels are also 0.02 m wide, but as the panels sit on vertical metal rails, this potentially seals or partially seals the cavity while exposing the unprotected vertical edges of both the left and right ACM panels. To approximate this condition a 0.02 m wide patch was imposed on the vertical gap between left and right panels. The ignition properties of the patch representing the gap was set to that for an unprotected panel edge i.e., 480$^{O}$C. Thus, the vertical gap was effectively sealed until the critical temperature for the panel edge was reached and the associated cell(s) were considered to be burnt through. In the BS 8414 Simulator, the intumescent is assumed to be activated when the air temperature between the solid barrier and ACM exceeds a critical value and after a prescribed delay time, to account for full activation of the barrier. A critical

temperature for the intumescent to be activated, of 260 $^{O}$C, is applied in the simulation work in [30]. This value is adopted in the BS 8414 model and a zero-delay time is assumed.

In the combustion model, the molecular structure of PE ($(C_2H_4)_n$) is used for all the combustible cladding materials but with the heat of combustion for the ACM core material for each test. For the wood crib fire, the effective wood molecular structure used in the analysis is $C_1H_{1.7}O_{0.83}$. A smoke to fuel ratio of 0.05 is used.

### 3.4 Mesh sensitivity analysis

The CFD predictions of the seven DCLG BS 8414 tests presented in this paper were performed using a computational mesh consisting of 300,348 (54×103×54) cells. A non-uniform mesh is utilised, with a cell size of 0.0125 m inside the cavity, 0.1 m inside the combustion chamber, 0.03 m near the ACM panel and 0.17 m at locations far away from the cladding system. To support this mesh selection, a mesh sensitivity study was performed for DCLG test 1 and test 7 (see Supplementary Material Section S4 for details). These two test cases were selected as they both represent fails of the cladding system and it was considered important to demonstrate that the fail status could be reliably predicted using the selected mesh budget. The mesh sensitivity study for DCLG test 1 involved four mesh budgets consisting of Mesh 1: 208,539, Mesh 2: 300,348, Mesh 3: 704,850 and Mesh 4: 1,019,424 computational cells. The mesh sensitivity study for DCLG test 7 used the relatively course Mesh 2 (300,348 cells) and the relatively fine Mesh 4 (704,850).

Most importantly, regardless of the mesh used, both DCLG test 1 and test 7 are predicted to fail due to the same failure criteria as observed in the test. Thus, whichever of the four investigated meshes is used, the main conclusions from the simulations match those of the test. Furthermore, the qualitative results relating to fire plume shape and burning/damage locations on the cladding are similar for all meshes and comparable with the experimental results.

Similarly, the predicted temperature curves at location 2 for both DCLG test 1 and test 7 are similar, irrespective of the mesh resolution, and reasonably close to the experimental results (see Fig S8(a) and S11(a)). The predicted curves for the cavity temperatures for all meshes and for both tests are also similar to each other for all meshes (see Fig S8(b) and S11(b)). However, these curves show a greater degree of discrepancy with the measured temperatures (this difference is further discussed in Section 4.2). Quantitively, for DCLG test 1, the time to fail based on the fire plume exceeding the top of the rig are close to the experimentally observed time of 360 s with prediction errors of -1.4%, 0%, -5.6% and -5.6% for Mesh 1 to Mesh 4 respectively. Similarly, the time for the Level 2 temperature rise to exceed 600 $^{o}$C are close to the observed time of 360 s, with prediction errors of 2.8%, 5.6%, -1.4% and -2.8% for Mesh 1 to Mesh 4 respectively (see Supplementary Material Section S4, table S2). Similar results are achieved for DCLG 7, with errors in the time for flames to extend above the rig being -10.8% and -18.7% for Mesh 2 and Mesh 3 respectively, and errors in time for the Level 2 temperature to exceed 600 $^{o}$C, being -11.4% and -22.1% (see Supplementary Material Section S4, table S2). Thus, while all the meshes produce similar temperature profiles and would lead to the same conclusions, particularly in terms of pass/fail of the cladding system and the corresponding causes, the Mesh 2 (300,348 cells) was considered appropriate for the purposes of this study, being a compromise between computational time and accuracy.

## 4. Simulation Results

In this section we present the numerical predictions produced by the BS 8414 model for each of the seven DCLG test cases. The presented results correspond to the numerical results recorded and reported in the actual tests and where possible, visual comparisons.

In total, 19 simulations were run using computers with a 4.0 GHz eight-core processor and 64 GB of memory. It required approximately 118 hours to simulate one scenario which passed the test involving a burning time of approximate 2000 s. Simulations for scenarios which failed the test would be terminated sooner, and so incur less simulation time.

### 4.1 Pass/fail status of the tested cladding systems

The fire performance criteria and classification methodology for the BS 8414 test are documented in BR 135 [8] according to the current ADB [4]. The start temperature $T_s$, is the mean temperature of any thermocouples at Level 1 during 5 minutes prior to the ignition of the wood crib fire. The start time $t_s$ is the time when the temperature recorded by any external thermocouple at Level 1 equals or exceeds a 200 $^{O}$C temperature rise above $T_s$ and remains above this value for at least 30 seconds. The observed $t_s$ in the tests and simulated values for each DCLG test are presented in Table 4. It is noted in Table 4 that the observed $t_s$ are different for each of the seven tests due to the variable HRR generated by the wood crib fires. Within the simulations, as a fixed HRR is used for the wood crib fires in all the simulations, this results in identical $t_s$ for all the simulations. The three failure criteria for a cladding system in the BS 8414 test, according to the criteria stated in BR 135, are:

**Criterion 1**: failure due to external fire spread being deemed to have occurred if the temperature rise above $T_s$, of any of the external thermocouples at Level 2, exceeds 600 $^{O}$C for a period of at least 30 seconds, within 15 minutes of the start time ($t_s$).

**Criterion 2**: failure due to internal fire spread being deemed to have occurred if the temperature rise above $T_s$, of any of the internal thermocouples at Level 2, exceeds 600 $^{O}$C for a period of at least 30 seconds, within 15 minutes of the start time ($t_s$).

**Criterion 3**: failure due to flame spread extending above the test apparatus at any time during the test duration.

Table 4. Values of $t_s$ (s) in the DCLG tests and corresponding simulations.

| | Test 1 | Test 2 | Test 3 | Test 4 | Test 5 | Test 6 | Test 7 |
|---|---|---|---|---|---|---|---|
| Measured (s) | 130 | 115 | 110 | 85 | 105 | 105 | 115 |
| Simulation (s) | 110 | 110 | 110 | 110 | 110 | 110 | 110 |

Presented in Table 5 is a summary of the experimental test and simulation results for the seven DCLG BS 8414 tests conducted by BRE. As seen in Table 5, the cladding systems in DCLG test 4, test 5 and test 6, passed the tests and all the other systems failed due to the flame spread extending above the test apparatus. The BS 8414 model correctly reproduced both the pass/fail results and identified the correct failure causes for all seven DCLG BS 8414 tests. The times to fail shown in Table 5, based on the flame criterion (Criterion 3), are when the flame reaches the top of the test facility in the experiments and simulations. Shortly after the failure of the two systems examined in Test 1 and Test 2 due to criterion 3, the two systems also fail due to criterion 1.

Table 5 Comparison of pass/fail results between tests and simulations.

| **DCLG test** | **Cladding materials** | **Results** | | **Note** |
|---|---|---|---|---|
| | | **Experiment** | **Simulation** | |
| **1** | PE; PIR | Fail due to Criterion 3 at approximately 360s | Fail due to Criterion 3 at approximately 360s | Criterion 1 was reached at 390s in the test and 410s in the simulation. The cavity temperatures are much lower than the failure criterion in both the test and simulation; |
| **2** | PE-Stone wool | Fail due to Criterion 3 at 275s | Fail due to Criterion 3 at approximately 360s | Criterion 1 was reached at 335s in the test and 410s in the simulation. The cavity temperatures are much lower than the failure criterion in both the test and simulation; |
| **3** | FR PE; PIR | Fail due to Criterion 3 at | Fail due to Criterion 3 at | Temperature rises at Level 2 external and cavity are below 600 |

| | | | | |
|---|---|---|---|---|
| | | approximately 1390s | approximately 1310s | $^{O}$C within 15 minutes in both the test and the simulation. |
| **4** | FR PE; Stone wool | Pass | Pass | Temperature rise at Level 2 exceeds 600 $^{O}$C 1280 s into the test, which is after the critical time requirement (within 15 minutes) for Criterion 1. The simulation has not predicted this peak temperature. The underprediction of this peak temperature does not affect the pass/fail result. |
| **5** | Limited combustibility mineral core; PIR | pass | Pass | Temperature rises at Level 2 (external and cavity) are below 600 $^{O}$C within 15 minutes in both the test and the simulation. |
| **6** | Limited combustibility mineral core; Stone wool | Pass | Pass | Temperature rises at Level 2 (external and cavity) are below 600 $^{O}$C within 15 minutes in both the test and the simulation. |
| **7** | FR PE; Phenolic insulation | Fail due to Criterion 3 at approximately 1525s | Fail due to Criterion 3 at approximately 1360s | Temperature rises at Level 2 (external and cavity) are below 600 $^{O}$C within 15 minutes in both the test and the simulation. |

### 4.2 Temperatures

When interpreting the presented temperature profiles, it is important to note that the start time (i.e., zero time in Fig. 5-7) for the BS 8414 experiments and corresponding simulations is not the time when the wood crib is ignited but is given by $t_s$, as defined in Table 4 [14]. It has been reported that the uncertainty in the measured experimental gas temperatures associated with

the Type K thermocouples required in the BS 8414 protocol is 5% [30]. Furthermore, it is important to note that within the model, the predicted thermocouple temperatures are simply approximated by the air temperature at the nearest cell centre corresponding to the thermocouple location. Without precise information concerning the thermocouples, any delay in thermocouple response (due for example to thermal inertia) is ignored.

In this section, the simulated temperatures for DCLG test 1, at prescribed critical thermocouple locations, are compared with the experimentally measured data. These critical thermocouple locations are 1035, 1029 and 1023 for the external thermocouples at Level 2 (see Fig 5a); 1034, 1028 and 1022 for internal cavity thermocouples at Level 2 (see Fig 5b) and 1005, 1003 and 1001 for external thermocouples at Level 1 (see Fig 5c). The three selected thermocouples, for each thermocouple group, correspond to the left, middle and right thermocouple of the five locations on the main wall shown in Fig. 1. Presented in Fig. 5 are the measured and predicted temperatures at each of the three thermocouple groupings at each location. For improved clarity, presented in the Supplementary Material (see Section S5) is an individual graph showing predicted and measured temperature at each individual thermocouple location.

The trends in the predicted external temperatures at Level 2 (see Fig. 5a and Supplementary Material Section 5, Fig. S15a, b and c) are comparable in magnitude and evolution with the experimental temperatures over time at each thermocouple location. Compared with the rapid rise of the measured external temperatures after 320 s (i.e., Level 2 external thermocouples), the measured cavity temperatures remain at a relatively low level due to the activation of the intumescent barrier (see Fig. 5b and Supplementary Material Section S5 Fig. S16a, b and c). From model predictions the internal horizontal intumescent fire barrier just above the chamber started activation at 65 s and, by 130 s, approximately one third of the barrier is activated (see Fig. 6). At the time of cladding system failure i.e., 360 s, most of the barrier under the top

panel has been activated. Up to approximately 320 s, the measured and predicted internal cavity temperatures at Level 2, broadly follow the same trends however it is noted that the precise activation criteria for the intumescent used in the DCLG tests is not known and was set in the modelling to activate when the intumescent surface temperature reached 260 $^{o}$C. Furthermore, the sudden rise in measured temperature at thermocouple location 1028 (centre thermocouple) after 320 s could be due to the external flame impinging on the vertical gap between the panels near the top of the facility (see Fig. 8 test 1) which is not precisely represented within the model (see Section 3.3). This could explain the observed 100 s delay in the predicted temperature rise at this location.

The predicted external temperature trends at thermocouple 1001 and 1005 at level 1, are in good agreement with the measured data (see Fig. 5c and Supplementary Material Section S5 Fig. S17a, b and c). The predicted temperatures at thermocouple 1003 (i.e., the centre thermocouple at Level 1) basically follow the measured trend; however, the measured data are considerably under predicted until 400s. The thermocouples at Level 1 are closer to the wood crib fire than those at Level 2. Therefore, the temperatures at Level 1 are significantly affected by the burning behaviour of the wood cribs. As there is significant variation in heat output for the wood crib fire between BS 8414 tests while within the simulations, the same HRRs are used for all simulations, the discrepancy between the measured and predicted temperatures at Level 1 is not surprising. However, the uncertainty in the predicted temperatures at Level 1 does not affect the reliability of the BS 8414 model as the predicted cladding fire spread and external temperatures at Level 2 for DCLG test 1 (Fig. 5a) and all other DCLG tests, are in good agreement with the test results.

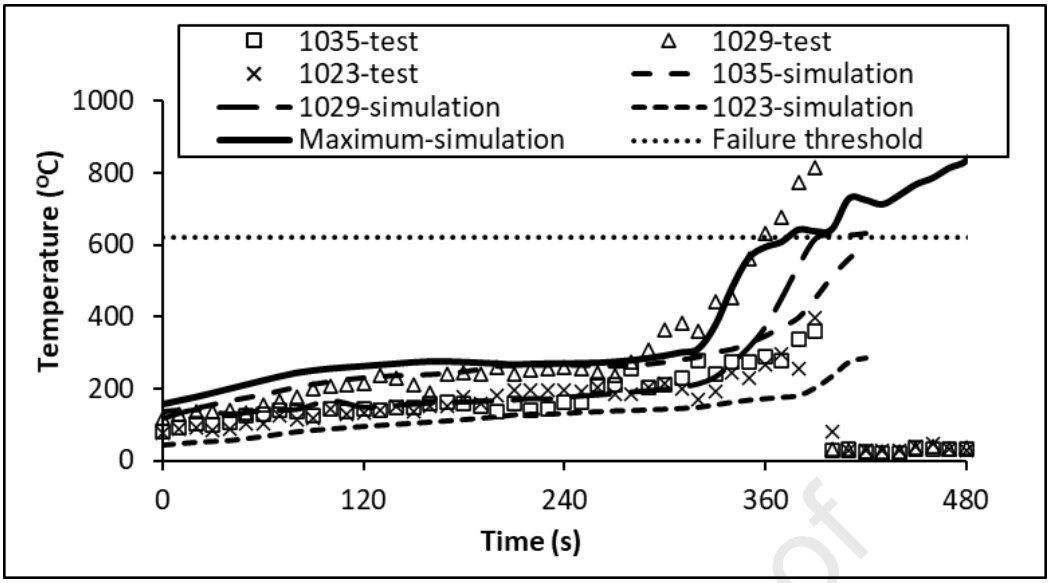


(a)

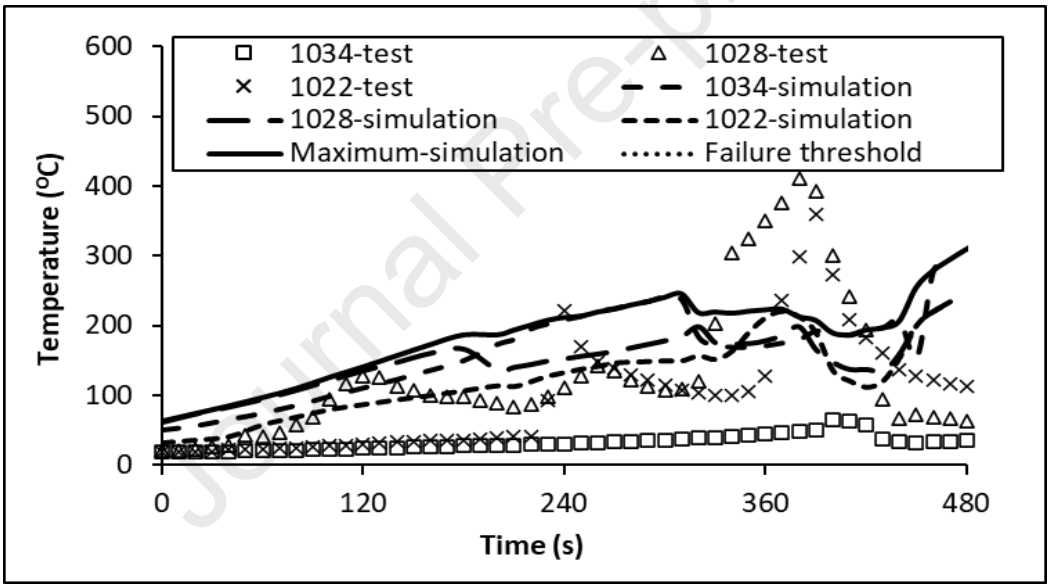


(b)

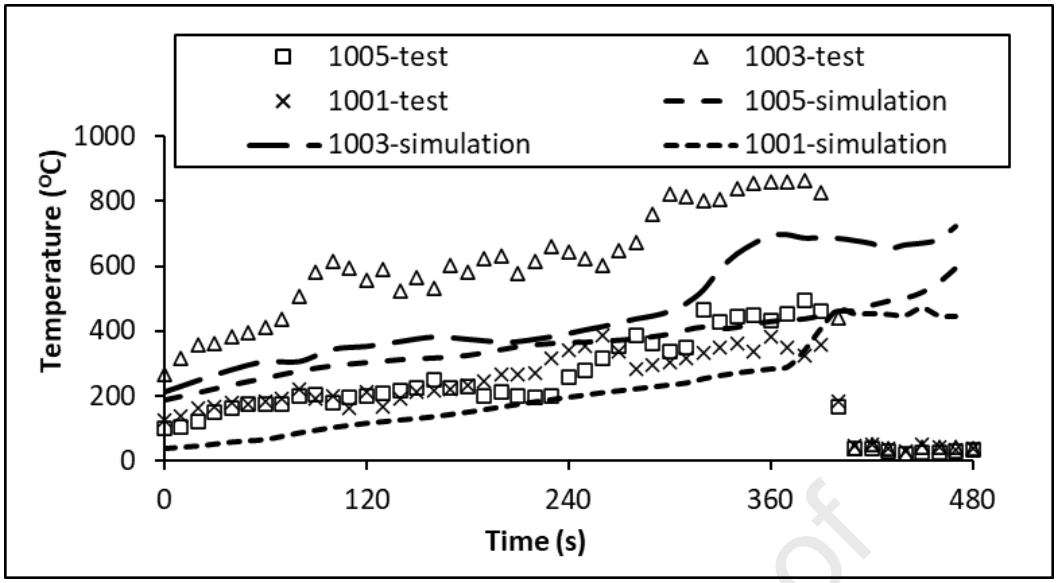


(c)

Fig. 5. Measured and predicted temperatures for BS 8414 DCLG test 1 at thermocouples (a) external level 2; (b) cavity level 2 and (c) external level 1.

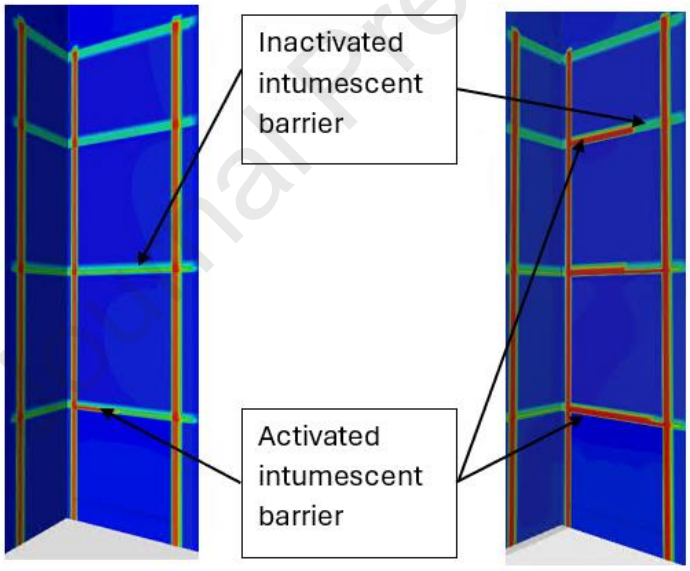


Fig. 6. Activated (red) and inactivated (green) horizontal intumescent barriers at 130 s (left) and 360 s (right) for BS 8414 DCLG test 1.

Criterion 1 indicates that if the rise of the maximum temperatures at the five external thermocouples of level 2, exceeds 600 °C, the cladding system is deemed to have failed. Similarly, if the rise of the maximum of temperatures at the five cavity thermocouples of level 2 exceeds 600 °C, the system is also considered to have failed. The experimental and predicted maximums of external and cavity temperatures at level 2 are compared as function of time for

the seven DCLG BS 8414 tests in Fig. 7. Basically, the predicted level 2 external and cavity temperatures follow the measured trends well, except for Test 4. For Test 4, the measured maximum external temperature rise, at level 2, slowly increases for the first 1200s and then begins to rise rapidly, exceeding the critical value of 600 $^{O}$C, between 1280s and 1330s. However, the cladding system is still deemed to have passed as the temperature breach occurred after the critical 15 minutes (i.e., 900s). The predicted maximum temperature closely follows the measured temperatures up to 1200s, but unlike the measured temperatures, there is no rapid rise, and the predicted maximum temperature remains below 600 $^{O}$C during the entire simulation period. Consequently, the simulation correctly predicted the assessment (pass) of this cladding system.

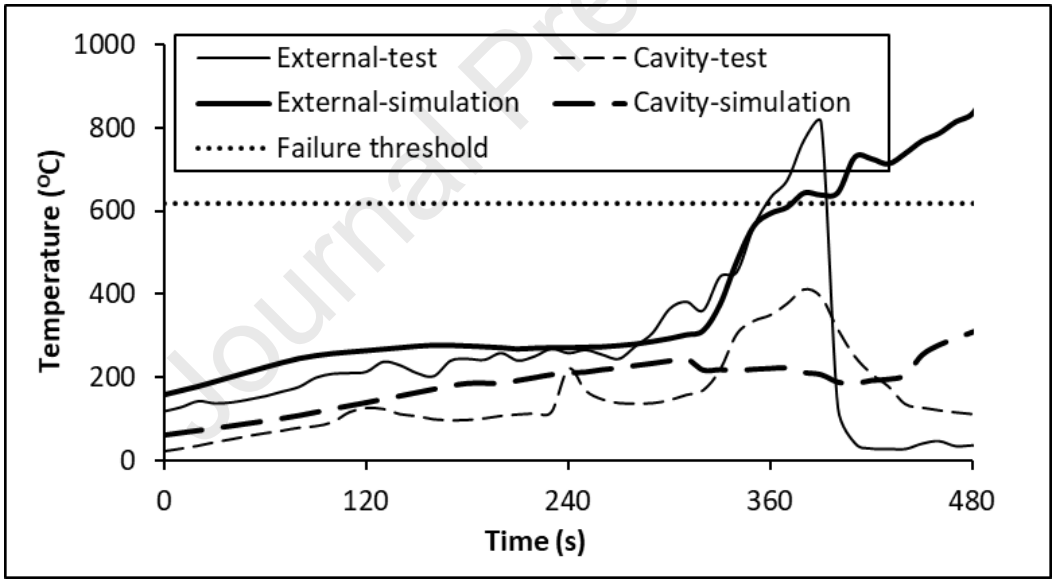


(a)

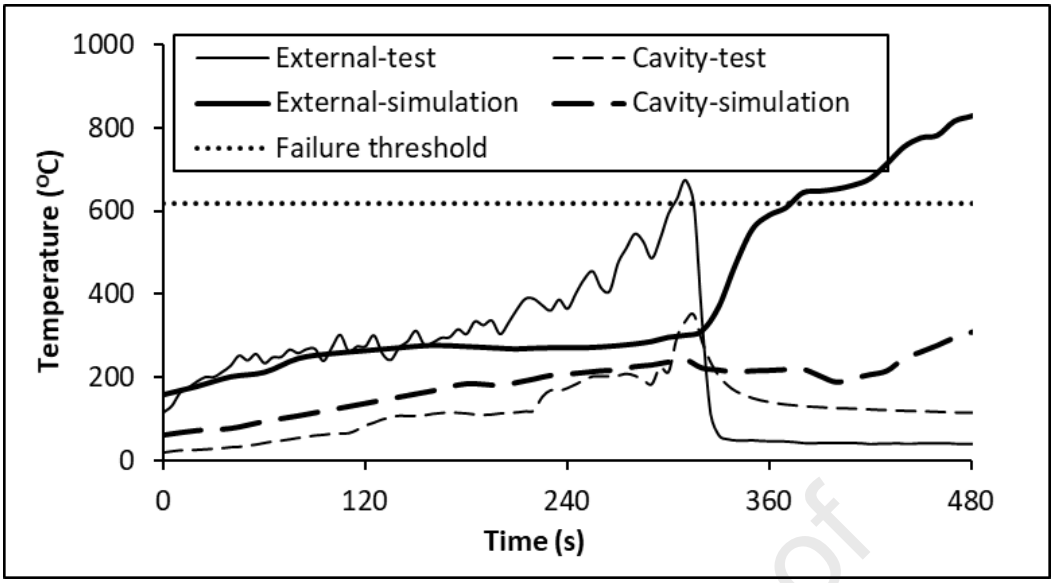


(b)

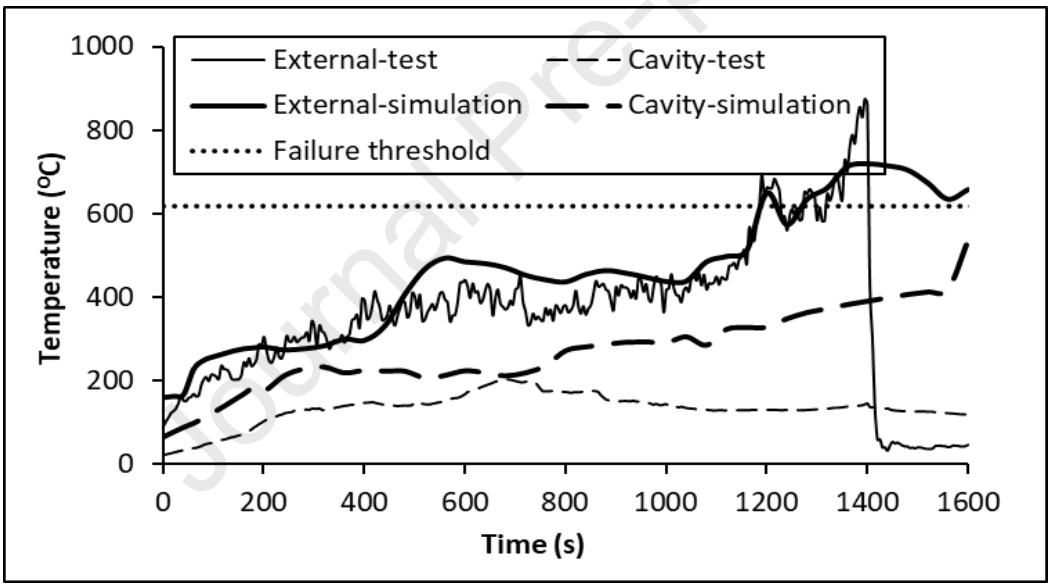


(c)

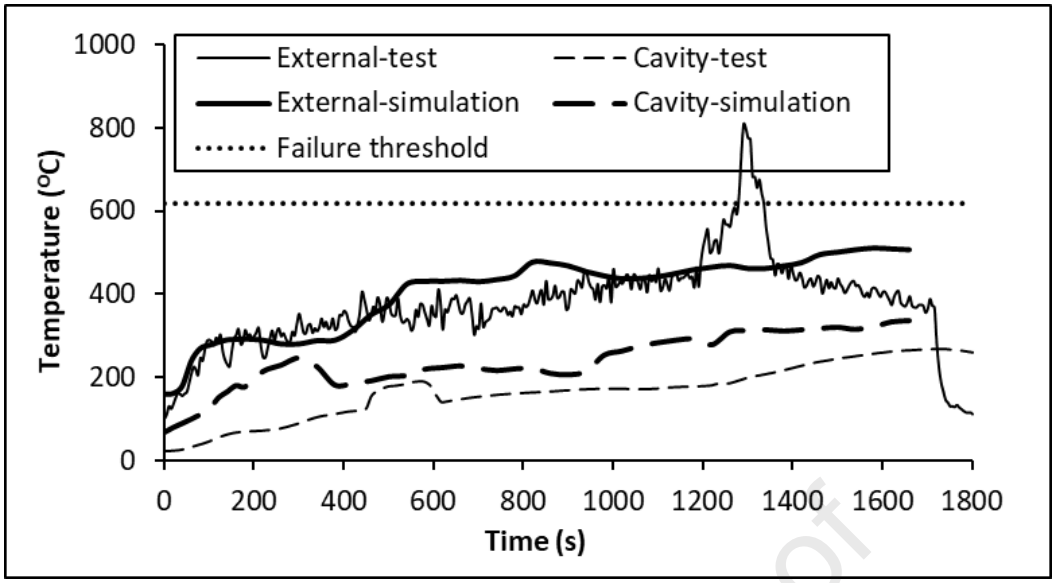


(d)

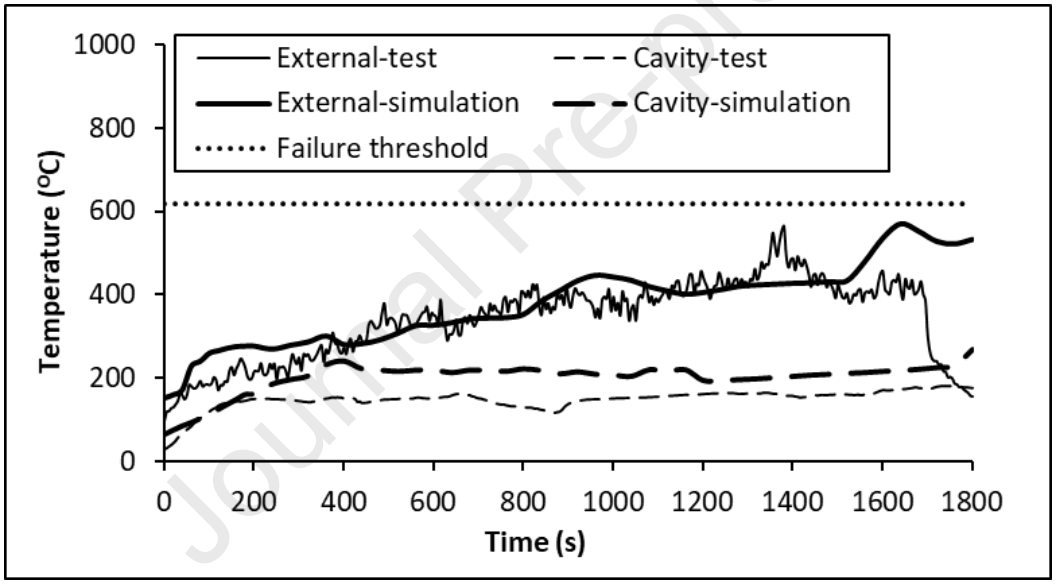


(e)

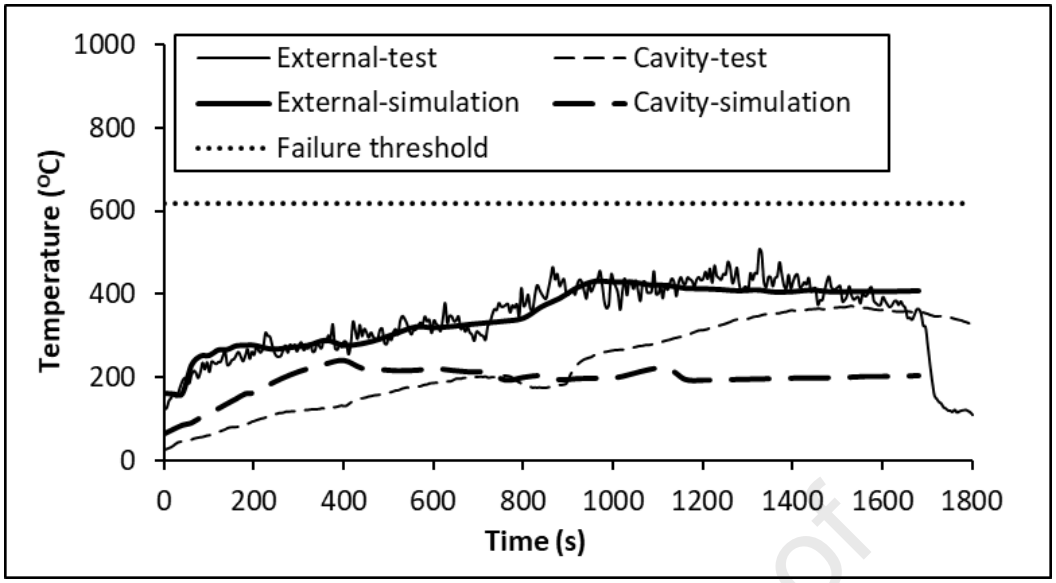


(f)

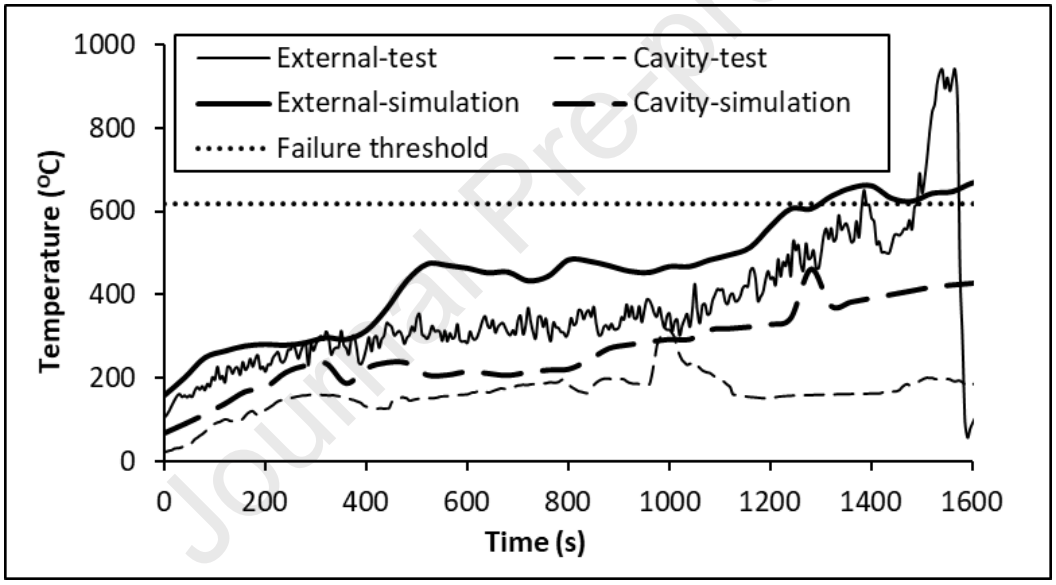


(g)

Fig. 7. Measured and predicted maximum level 2 temperatures on main wall (a) DCLG BS 8414 Test 1; (b) Test 2; (c) Test 3; (d) Test 4; (e) Test 5; (f) Test 6 and (g) Test 7.

### 4.3 Flame height

The height of the fire generated by the cladding system is used as one of the pass/fail criteria for DCLG BS 8414 tests, referring to BR 135. The cladding system failures in DCLG BS8414 Test 1, Test 2, Test 3 and Test 7 are all due to the visible flame extending above the test facility, within 1800s. Therefore, the predicted flame heights are compared with the observations during these tests in this section. In Fig. 8, the visible flames predicted by the simulations are represented by a temperature iso-surface of 525 $^{O}$C, the minimum temperature of a flame that

can be considered visible [27]. This flame criterion is consistent with the observation based on pool fire experiments that the mean flame height of pool fires for normal atmospheric conditions corresponds to a temperature rise on the plume axis of 500 $^{O}$C above ambient [56]. The times noted in Fig. 8 are the instances when failure Criterion 3 is reached for DCLG test 1, Test 2, Test 3, and test 7, and are the instances at which the flames are at their highest height during the experiments/simulations for the other tests. Note, as with the temperature profiles presented in Fig. 5 and Fig. 7, the times for the flame envelopes presented in Fig. 8 are adjusted using the $t_s$ values in Table 4. In Test 1, 2, 3, and 7, in which the corresponding cladding systems fail, the flames lean to the corner formed by the wing wall and the main wall and reach the top of the test facility. The simulations of these tests reproduce the observed flame behaviours and shapes. Furthermore, in DCLG Test 4, 5, and 6, the flames reach the top the of middle ACM panel in both the experiments and simulations.

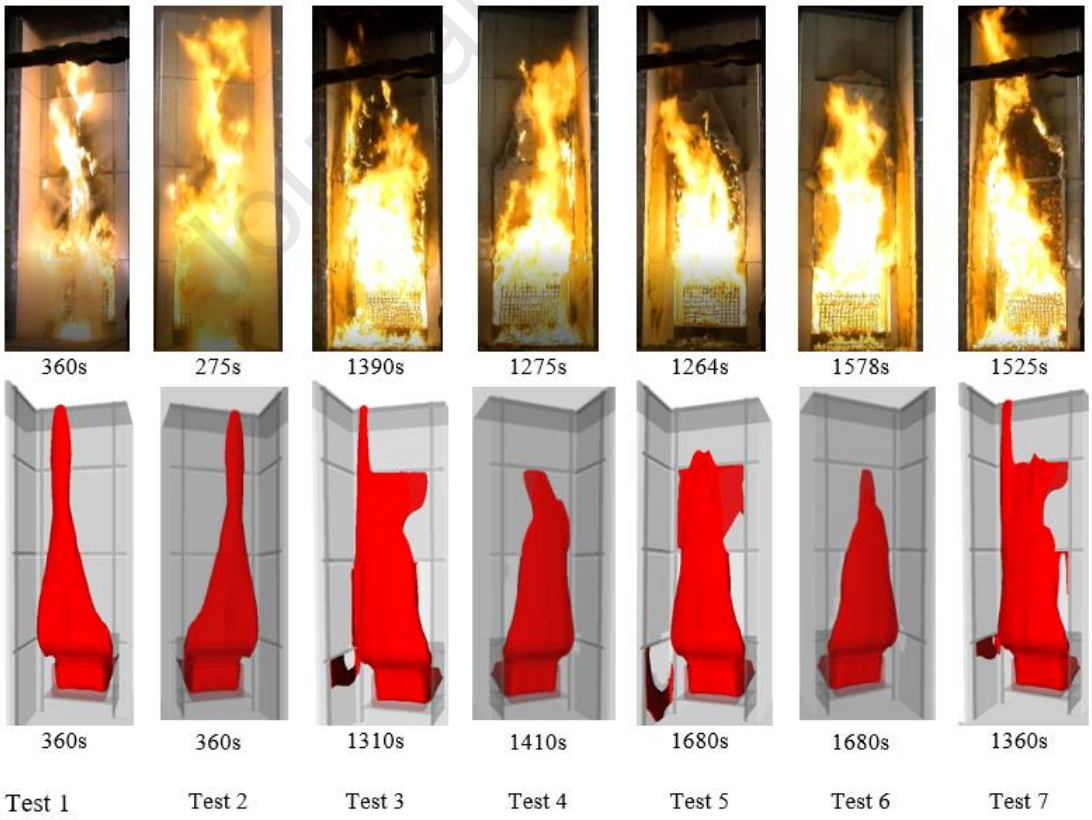


Fig. 8. Observed and simulated flames (where the simulated visible flame envelopes are defined using a 525 $^{O}$C temperature iso-surface).

Presented in Table 6 is a quantitative comparison between experimental results and model predictions for the time for the visible flame to extend beyond the top of the test facility and the rise of the external level 2 temperature to exceed 600 $^{O}$C for the four tests that failed i.e., Test 1, 2, 3 and 7. These are critical events in BS 8414 tests and so it is important that the model is capable of providing a reasonable prediction of these events. As seen in Table 6, the prediction errors are between 0% and 30.9% for the flame related events and between 0.1% and 24.6% for the temperature related events. The maximum prediction error is observed in the simulation of DCLG test 2, in which the cladding system failed as early as 275 s. It is noted that DCLG test 2 (comprising of ACM with PE core and stone wool insulation) failed 85 s earlier that DCLG test 1 (comprising of ACM with PE core and PIR insulation). This anomaly is likely due to the variability in the HRR for the wood crib fire. As the simulations for all seven DCLG tests use the same HRR curve for the wood crib fire, this results in the relatively large error of 30% for DCLG test 2. Furthermore, this observation supports the criticism of the variability of the HRR produced by the wood crib fire used in the BS 8414 test (see Section 5.4).



Table 6. The time for the flame height to exceed the height of the test rig and time for the level 2 external temperature rise to exceed 600 $^{O}$C and relative prediction errors.

| **DCLG test** | **Time for flame to reach the top of the test facility (s)** | | **Simulation error (%)** | **Time for level 2 temperature rise to exceed 600 $^{O}$C (s)** | | **Simulation error (%)** |
|---|---|---|---|---|---|---|
| | **Experiment** | **Simulation** | | **Experiment** | **Simulation** | |
| **1** | 360 | 360 | 0 | 360 | 380 | 5.6 |
| **2** | 275 | 360 | 30.9 | 305 | 380 | 24.6 |
| **3** | 1390 | 1310 | 5.8 | 1190 | 1195 | 0.4 |
| **7** | 1525 | 1360 | 11.8 | 1490 | 1320 | 11.4 |

### 4.4 Damage to the cladding systems

The damage to the cladding systems in the seven tests after the fire termination have been reported in [14]. The model predictions of the damage to the ACM panels are compared with

the experimental results in this section. The final burning/burnt locations predicted in the simulations are at a derived termination time for each test. The derived termination time is defined as:

- For a cladding system passing the BS 8414 test, the derived termination time is 1800s, as there were almost no visible flames in the tests after this time.
- For a cladding system failing the test, the derived termination time is the sum of the time to fail in the simulation and the time difference between the termination time and the time to fail in the experiment.

The derived termination time in the simulation of DCLG BS8414 test 1 is 395 s. Presented in Fig. 9 is a comparison of the burnt locations in the test and the predicted burnt/burning locations at the derived termination time. The simulation of DCLG test 1 produces a similar size of the ACM burnt off area marked with dashed circles in Fig. 9a. A large area of the external skin of the ACM panel melted away exposing its PE core in the test, while the predicted burning locations (marked by dots) at the derived termination time are comparable. After the ACM panel was removed, a large area of the PIR insulation was seen to be damaged by the fire in the experiment (marked with a dashed circle in Fig. 9b). A similar area of the PIR damage (marked with dots) is predicted in the simulation at the derived termination time.

It is reported that almost no activation of intumescent occurred on the wing wall and at the top barrier on the main wall in the DCLG BS 8414 test 1 [14]. No intumescent activation occurred at these locations during the simulation. It is also reported that the intumescent on the two bottom horizontal barriers on the main wall were either burnt off or completely activated in the test. While the bottom barrier was completely activated (red barrier), only two thirds of the intumescence on the second barrier was activated in the simulation. Furthermore, in the test,

the intumescent was partially activated on the third barrier but was predicted to be fully activated in the simulation. The simulation reproduces reasonably similar intumescent activation state at 395 s (red represents activated intumescent while light blue represents inactive intumescent) as seen in Fig. 9b.

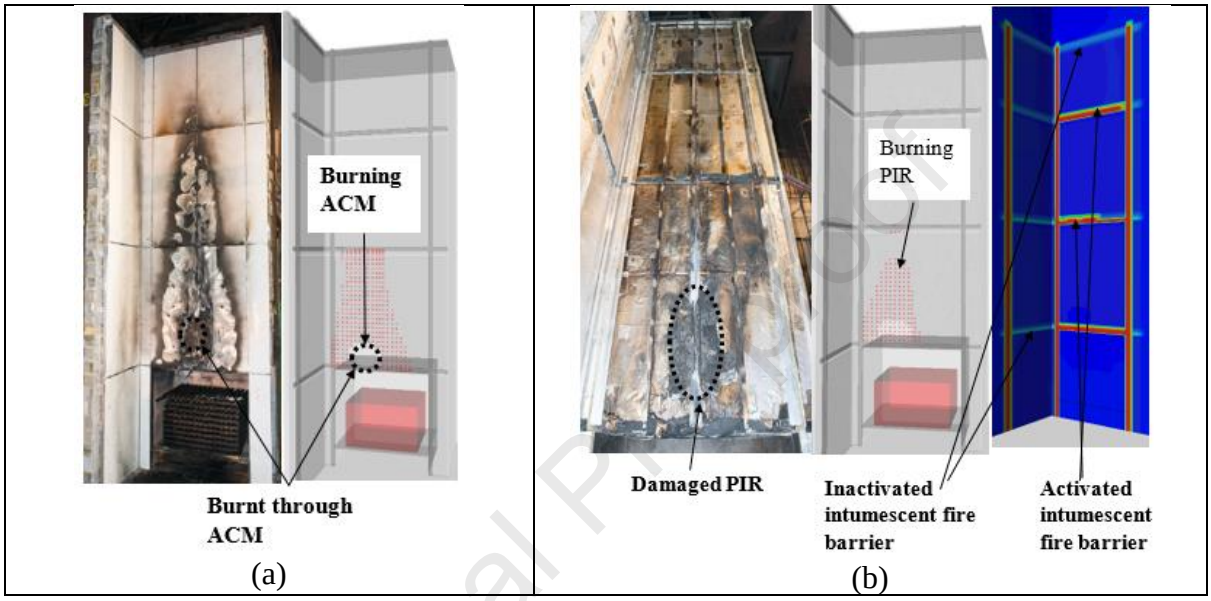


Fig. 9. DCLG BS 8414 test 1 (a) the final burnt off ACM (dashed circle) in the test, the burnt off (dashed circle)/burning ACM (red dots) locations at the derived termination time of 395s in the simulation; (b) the damaged PIR in the test, burning locations of PIR (red dots) and activation state of barrier intumescent at 395s in the simulation.

Figure 10 compares the predicted and actual damage to the cladding systems for other DCLG BS 8414 tests. The derived termination times in the simulations to these tests are shown in the figure. The burnt off locations of the ACM panels (the white/light-grey area) in the simulations are comparable with the observations from the experiments for all the tests.


Fig. 10. Burnt off ACM panel in the experiments and the predictions (lighter grey area) at the derived termination time of fire in the simulations (red dots represent actively burning locations).

## 5. Further Analysis

In this section we present additional numerical predictions produced by the BS 8414 model for each of the seven DCLG test cases. The presented results explore the impact of fire parameters on test performance not explicitly considered in the standard BS 8414 test.

### 5.1 HRRs from individual materials

HRR is a very important characteristic for fires. Unfortunately, the BS 8414 standard [7] does not require the HRR of the test to be measured or assessed. In contrast, the BS 8414 model can identify the burning rates of each component of the cladding system material involved. As an example, the predicted HRRs from the simulation of DCLG test 1, using the BS 8414 model,

are presented in Fig. 11. With the given wood crib HRR (shown in Fig. 5), the zero time in Fig. 11 is 110 s after the ignition of the crib fire, when the rise of the level 1 temperature reaches 200 $^{O}$C. The predicted peak HRR for DCLG test 1 is 9.2 MW at approximate 720 s, which is made up of contributions from the burning of PE, PIR and wood crib as follows 6.1 MW, 0.6 MW and 2.5 MW respectively. For comparison, the simulation reported in [30] of DCLG test 1 produced a peak HRR of approximately 7.6 MW at approximately 480 s. The maximum HRR contributed by the cladding is 6.7 MW in this study, compared with approximately 4.5 MW in [30]. The main contribution to the predicted peak HRR is the PE within the ACM, which is more than 10 times greater than the contribution from the PIR insulation.

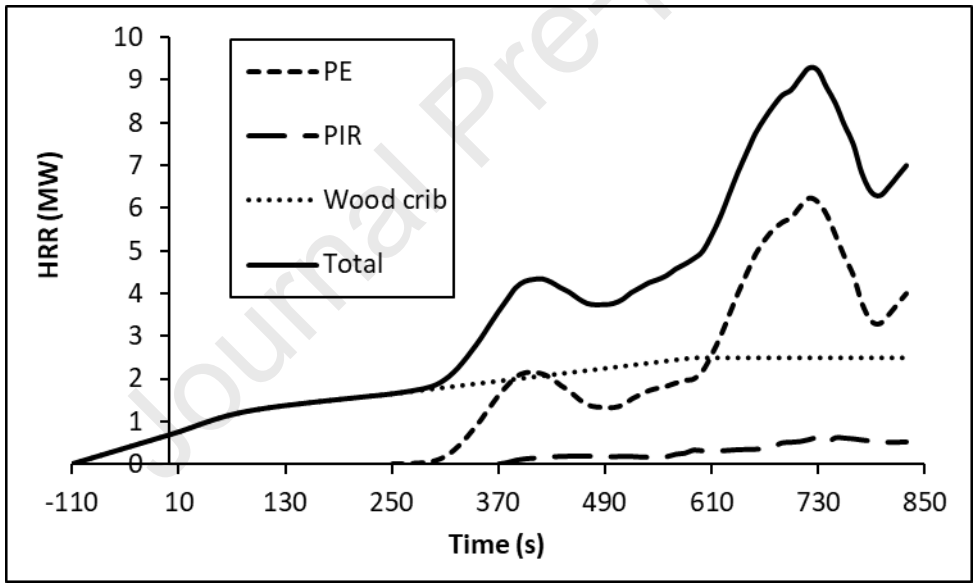


Fig. 11. Predicted HRRs in the simulation of DCLG BS 8414 test 1.

### 5.2 Impact of cavity size

In the DCLG BS 8414 tests, the cavity between the ACM panel and the insulation is approximately 0.05 m [14]. In the ACM cladding system used in the Grenfell Tower, there was a 0.156 m cavity space [3]. How does cavity size impact the vertical and lateral fire spread in a cladding system? Using the BS 8414 model the impact of cavity size can be investigated. To

demonstrate the impact two scenarios are considered. In one scenario, the original DCLG BS 8414 test 1 (i.e., ACM with PE core and PIR insulation), with a cavity size of 0.05 m is used as a base case, while a second scenario, which has an identical setup to test 1 but with a cavity size of 0.15 m is considered.

The two cladding systems are predicted to fail at almost the same time (360 s) due to the flame rising beyond the top of the facility (Criterion 3). Up to this time, there are no significant differences in the external and cavity internal temperatures for both cavity widths (see Supplementary Material, Section S6 and Fig. S18). However, the BS 8414 model can continue the simulation to further investigate the fire development characteristics. For some time after the cladding system has failed (i.e., at 360 s) the average internal cavity temperature in the larger cavity exceeds that of the smaller cavity (see Supplementary Material, Fig. S18b). Furthermore, depicted in Fig. 12 are the burning and burnt-off locations in the two scenarios at 730 s, long after both systems are predicted to fail (i.e., 360 s). As seen in Fig. 12, almost all the ACM panels on the main wall are burnt off (white area) in scenario 2 (0.15 m cavity) at 730 seconds; but the burnt off area in scenario 1 (0.05 m cavity), is approximately only two thirds of that for scenario 2. The simulations suggest that for the case with the larger cavity (i.e., scenario 2) the fire spreads more rapidly on the cladding both vertically and laterally than for the case with the smaller cavity (i.e., scenario 1).

To further explore this behaviour, the lateral and vertical flame spread rates on the cladding for both narrow and wide cavities are estimated from the simulations (see Supplementary Material, Section S6 for details). The flame spread is determined by the location of the predicted combustion front. However, these flame spread rates are difficult to quantify as they vary across the entire face of a panel and potentially from panel to panel. Furthermore, when estimating both the lateral and vertical flame spread rates, the lowest panel locations (i.e., panels 1C and 1D in Fig. 1) are not considered as the flame spread rates on these panels are

expected to be dominated by the spill plume arising from the fire chamber immediately below the panel.

To characterise the lateral flame spread rate associated with the different cavity sizes, the centre line across the middle panels on the main wall (i.e., panels 2C and 2D in Fig. 1) were selected. This line is located 5.6 m above the floor (3.6 m above the top of the fire chamber) representing a length of 2.04 m. To characterise the vertical flame spread rate, a vertical line on the centre top two panels of the main wall (i.e., panels 2C and 3C in Fig. 1) 0.2 m to the left of the middle vertical panel gap was selected.

For the narrow cavity (0.05 m), the average lateral flame spread rate on the cladding was estimated to be 0.010 m/s while for the wide cavity it was estimated to be 0.013 m/s i.e., 30% faster (see Supplementary Material, Section S6 for details). In addition, it is important to note that the cladding at the selected horizontal line first ignites after 460 s in the wide cavity and 483 s in the narrow cavity. Thus, in the wide cavity case, the lateral flame speeds are measured at a time of lower HRR from the wood crib fire. For the narrow cavity (0.05 m), the average vertical flame spread rates on cladding panels 2C and 3C (see Fig. 1) were estimated to be 0.007 m/s and 0.006 m/s respectively while for the wide cavity (0.15 m), they were estimated to be 0.008 m/s (i.e., 14% faster) and 0.008 m/s (i.e., 33 % faster) respectively (see Supplementary Material, Section S6 for details).

Comparing the relative magnitudes of the predicted vertical and lateral flame spread rates is not straightforward. The lateral flame spread is progressing in two directions i.e., left and right, whereas the vertical is progressing essentially in a single direction i.e., upwards. Furthermore, the cladding along the horizontal line is first ignited some 230 s after the vertical line is first

ignited, and virtually all of the horizontal line is covered in the flames from the spill plume for the entire duration of the measurement, while the vertical line is only progressively exposed to flame.

The faster lateral and vertical fire spread rates for the wide cavity compared to the narrow cavity case is the result of the higher average cavity temperatures in the wider cavity after the cladding system fails i.e., 360 s (See Supplementary Material Section S6 and Fig. S18b). Thus, while both the narrow and wide cavity case are determined to fail the BS 8414 test at around the same time, and for the same reason, the wider cavity case presents a significantly more hazardous situation, as both the average lateral and vertical flame spread rates are greater. Thus, the cladding fire will spread more rapidly to other parts of the building exterior with a wider cavity. These findings are important as they help to understand the observed fast lateral and vertical fire spread in the Greenfell Tower fire [3].

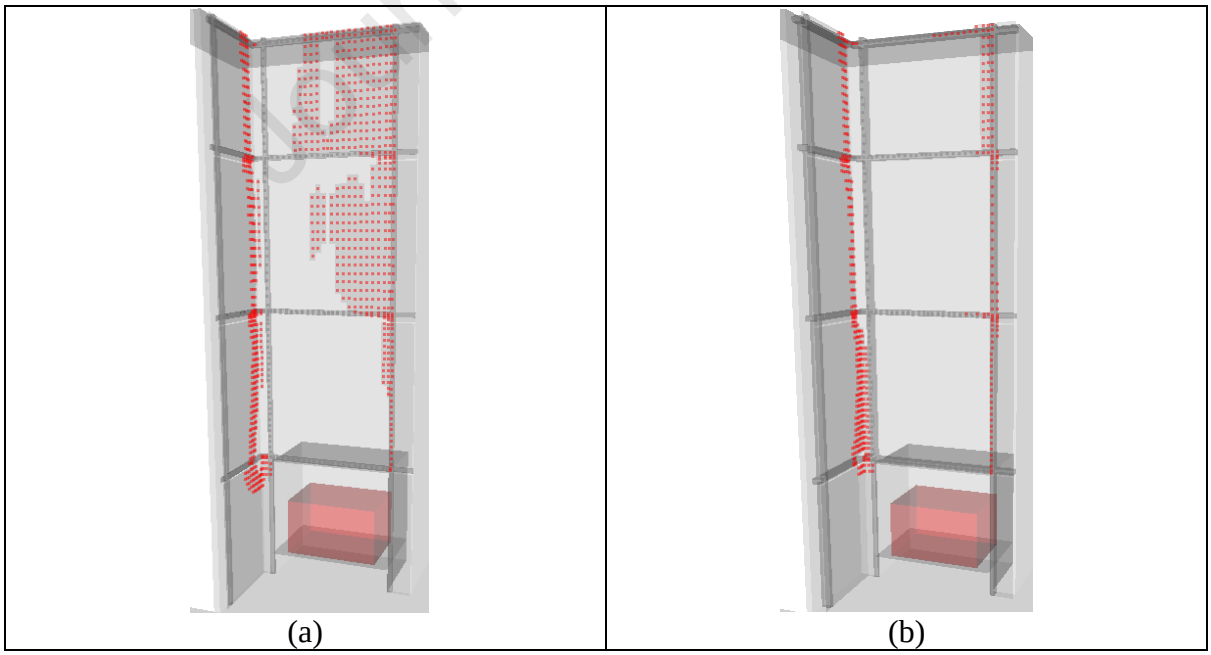

(a) (b)

Fig. 12. Predicted burning locations (red dots) and burnt off ACM (lighter grey areas) at 730s with a cavity size of (a) 0.05 m and (b) 0.15 m.

### 5.3 Impact of a reduction in mass of ACM core material on the developing fire

As seen in Fig. 8, some of the melted cladding materials dripped onto the ground during the fire experiments. In this section, the impact of reducing the mass of PE in the ACM panel (for example, due to dripping) is analysed based on DCLG BS 8414 test 1. Three fire scenarios with the same set up as for the simulation of DCLG BS 8414 test 1 are considered, but with adjusted HRR curves resulting from the reduced mass of available PE (i.e., less the mass assumed to be lost due to dripping). The reduction of HRRs of PE in the three scenarios is 0%, 20% and 30% of the HRR that is used in the simulation of the original DCLG BS 8414 test 1.

In the simulation of DCLG BS 8414 test 1, the cladding system fails at 360s due to the flame extending beyond the test facility (criterion 3). At this time, the predicted fire plume in the scenarios with a 20% or 30% reduction in the mass of PE are far from the top of the test facility (Fig. 13). Nevertheless, with a 20% or 30% reduction in the mass of PE , the cladding system is still predicted to fail due to criterion 3. However, the times for the flame to reach the top of the test facility in these two scenarios are 390 s and 420 s, representing a delay of 30 s and 60 s respectively compared with the scenario without any PE loss. This study shows that even with a 30% reduction in the mass of the available PE , the cladding system in the DCLG test 1 will still fail with a delay of just approximately 60 s. The dripping of melted PE core material is a complex phenomenon that can have several effects on fire development. The most obvious impact on the developing fire is that the dripping constitutes a loss of available fuel, thus, the dripping of PE core material noted in the Grenfell fire is likely to have slowed the upward vertical (and lateral) rate of fire spread slightly, but even a loss of as much as 30% of the available core material would not have prevented the disaster from occurring. However, dripping fuel could ignite in a spill plume or flame sheet as it is falling and hence contribute to the flame sheet, it could also adhere/solidify to lower segments of the rainscreen cladding –

resulting in easier ignition at some later stage of the fire, and could, if the drips are able to keep burning as they fall, result in enhanced downwards fire spread.

It is acknowledged that the extremely complex dripping phenomenon has not been adequately modelled in the current simple analysis. The main simplification of the current approach is that the impact of the molten fuel droplets in redistributing fuel, and the possibility of burning droplets spreading combustion to regions remote from the main fire, has not been represented. However, the analysis highlights that even if the PE core material in the investigated scenario is greatly reduced, it still fails to pass the BS 8414 test.

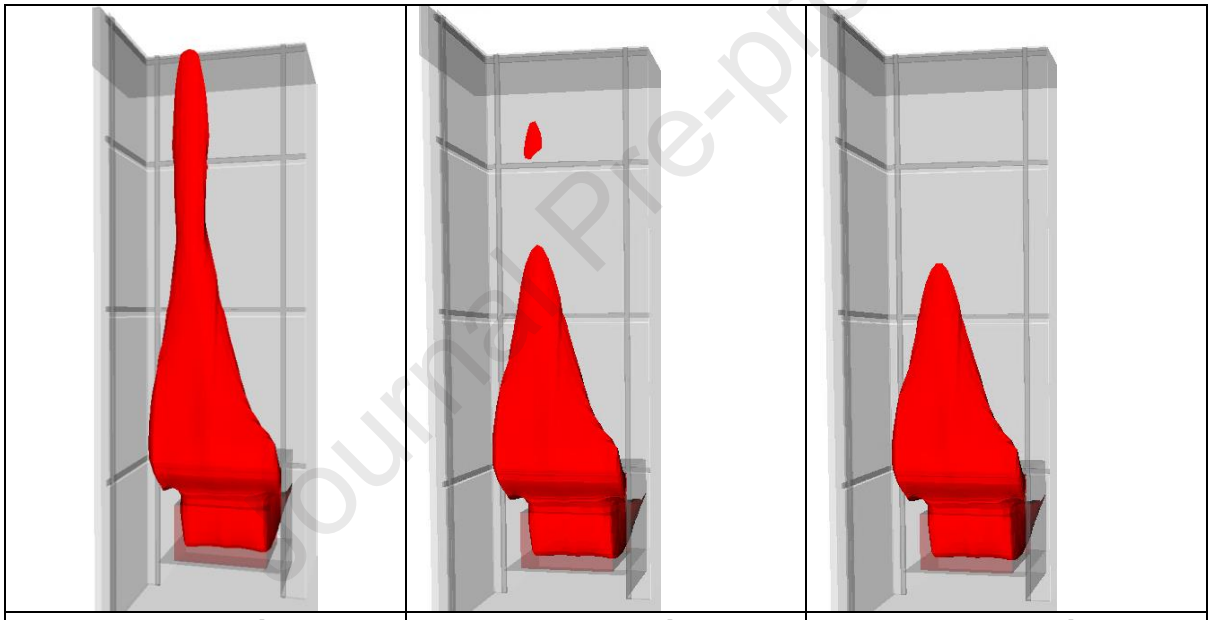


Fig. 13. Predicted fire plumes at 360s associated with loss of fuel (PE) from the ACM panels equivalent to 0%, 20% and 30% of the available fuel mass in simulations of DCLG BS 8414 test 1

### 5.4 Impact of wood crib fire

In the BS 8414 test standard [7], the peak HRR of the wood crib fire is stipulated to be between 2.5 MW and 3.5 MW. A HRR curve with a peak value of 2.5 MW is utilised for the wood crib fire in the simulations presented in this study. In this section, the influence of the peak heat output of the wood crib fire on the outcome of BS 8414 tests is investigated. This analysis is

conducted for the DCLG BS 8414 test 4 with FR PE as the ACM core and stone wool as the insulation, which passed the experimental test. Three wood crib fire scenarios with peak HRRs of 2.5 MW, 3.0 MW and 3.5 MW are investigated. As seen in Section 4 (see Table 5), with a peak HRR of 2.5 MW for the wood crib fire, the simulations agree with the experimental results and predict that the cladding system passes the BS 8414 test. In contrast, the same cladding system will fail at 1250 s and 820 s due to the fire plume extending beyond the top of the test facility (criterion 3) if the wood crib fires are 3.0 MW and 3.5 MW respectively (See Fig. 14). This means that the cladding system in the DCLG BS 8414 test 4 would fail the test if the HRR peak of the wood crib fire was 20% higher, but still within the suggested range in the BS 8414 standard. This suggests that given the natural variation in HRR produced by wood crib fires utilised in the BS 8414 test, a cladding system could pass or fail depending on the natural variation in HRR.

Dréan et al. [30] found that the permitted variability in HRR for wood crib fires in BS8414 tests (i.e., 2.5 MW, 3.0 MW and 3.5 MW) does not significantly influence results achieved for the DCLG test 1. They reported that HRR curves from the burning of the cladding at various wood crib HHRs appear to be only time shifted, with close peak values. While this is a valid conclusion for DCLG test 1, it is not a valid conclusion for BS 8414 testing in general. It should be noted that, as DCLG test 1 failed (significantly), it is unlikely to be sensitive to the upper and lower end of the permitted HRR for the wood crib fire. However, as DCLG test 4 passed, it is particularly sensitive to the upper end of the allowable HRR for the wood crib fire. The finding from the study reported in this paper brings into question the repeatability of the BS 8414 test and hence its suitability as a standard.

It is suggested that the wood crib in the BS 8414 test be replaced by a gas burner which would improve the repeatability of the test.

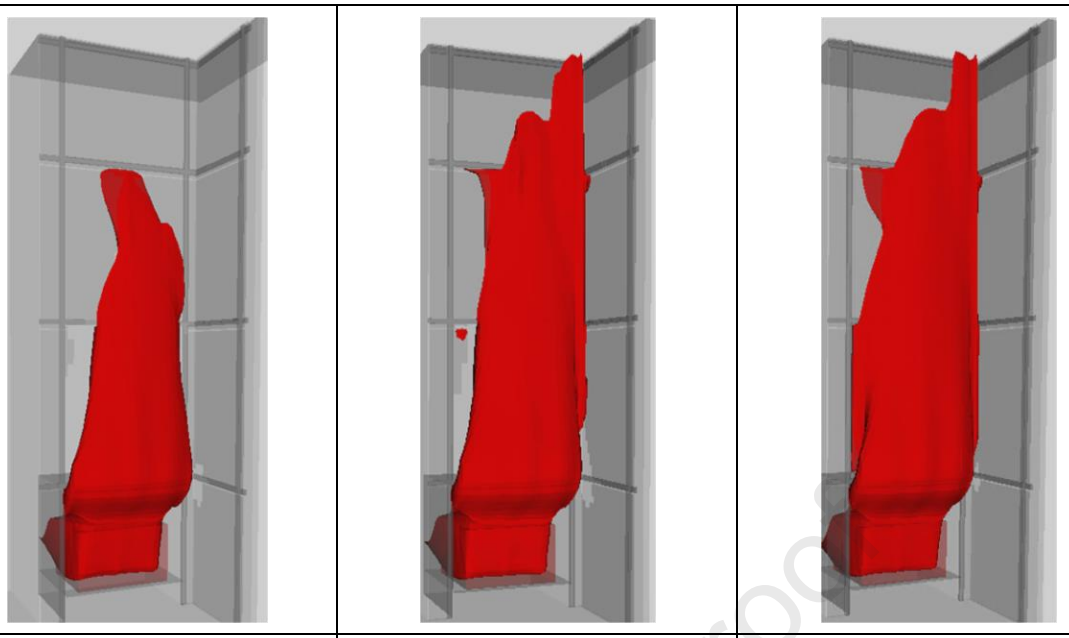

| (a) maximum extent of fire plume | (b) fire plume extent at time of failure (1250 s) | (c) fire plume extent at time of failure (820 s) |
|---|---|---|

Fig. 14. Fire plumes in simulations of DCLG BS 8414 test 4 with a peak wood crib HRR of (a) 2.5 MW ; (b) 3.0 MW and (c) 3.5 MW.

### 5.5 Impact of barriers and intumescent

The section considers the impact of the fire barriers on fire spread, and what are the implications of incorrectly installing a fire barrier or if the attached intumescent is dysfunctional. The impact of this deficiency on the cladding fire development is demonstrated by simulating a scenario similar to the DCLG BS 8414 test 1 (i.e., PE ACM with PIR insulation) but with a cavity size of 0.15 m and with some changes to the representation of the modelled barriers/intumescent as shown in Fig. 15. In total, four scenarios are considered;

- Scenario BI1 has fully installed barriers/intumescent as in DCLG BS 8414 test1 (Fig. 15a);
- Scenario BI2 is the same as Scenario BI1 but removing three horizontal barrier rows on the main wall (Fig. 15b);

- Scenario BI3 is the same as Scenario BI1 but the intumescent on the three barrier rows on the main wall is inactive (see Fig. 15b for the locations of the inactive intumescent rows);
- Scenario BI4 is the same as Scenario BI1 but part of the vertical barrier above the chamber is removed (near the corner, Fig. 15c).

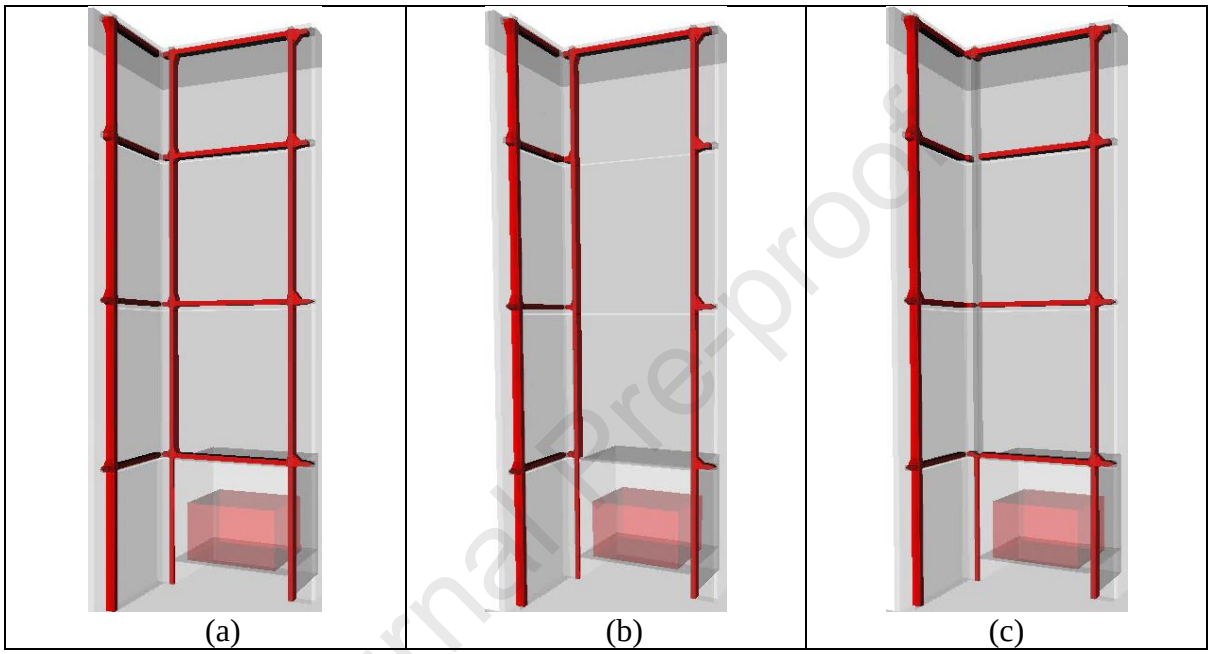


Fig. 15. The four barrier scenarios (a) with full barriers/intumescent (BI1); (b) with the absence of three horizontal barrier rows (BI2) or with inactive intumescent at three horizontal barrier row (BI3) and (c) with the lack of a vertical barrier at the wing-main wall junction (BI4).

The change in the external temperature at level 2 caused by the various barrier states are moderate. In scenario BI1, the predicted rise of level 2 temperatures above 600 $^{O}$C occurs at 370 s. With the removal of the vertical barrier, the time for scenario BI4 is the same as that in scenario BI1. The critical time for scenario BI2 (with the removal of the horizontal barriers) is 345 s (i.e., 25 s earlier) and for scenario BI3 (with the inactive barrier intumescent ) is 340 s (i.e., 30 s earlier) (see Fig. 16a).

However, the barrier/intumescent states have a more significant impact on the cavity temperatures. The predicted level 2 cavity temperatures are again similar in scenarios BI1 and

BI4 (see Fig. 16b). In scenarios BI1 and BI4, the predicted time for the rise of the level 2 cavity temperatures, above 600 $^{O}$C, is 570 s, while in scenario BI2 and BI3, the time is 390 s (i.e., 180 s earlier) and 500 s (i.e., 70 s earlier) respectively. The absence of horizontal barriers, or failure for the intumescent to activate, causes a faster vertical and lateral fire spread.

It is noted that these four cases are predicted to all fail the BS 8414 test due to the flame height exceeding the top of the rig (criterion 3) at 360 s, 335 s, 335 s and 362 s for scenarios BI1, BI2, BI3 and BI4 respectively.

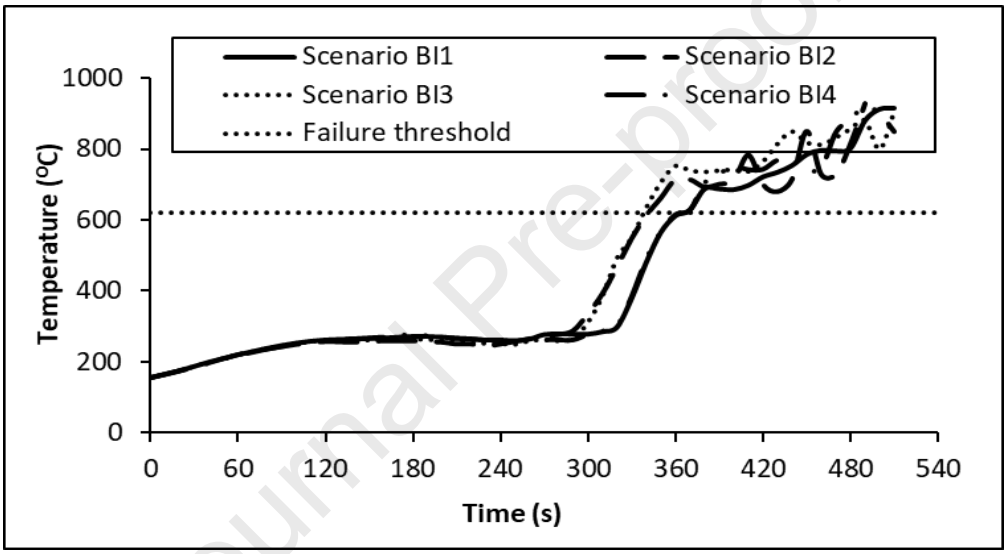


(a)

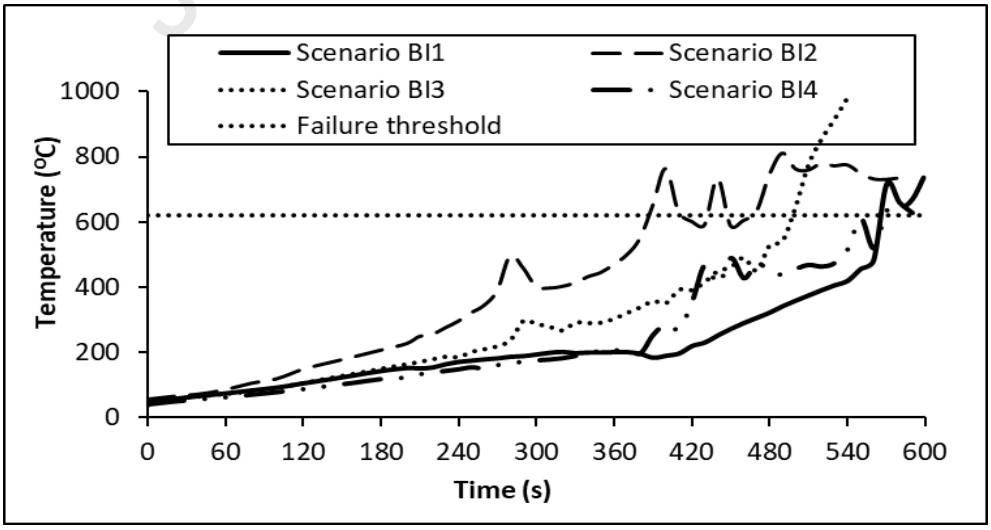


(b)

Fig. 16. Maximum level 2 temperatures for the four barrier-intumescent scenarios (a) external temperatures and (b) cavity temperatures.

Presented in Fig. 17 are the final burning locations on the ACM panel at 600 s for each of the four barrier scenarios while presented in Fig. 18 are the burning locations on the insulation. The importance and effectiveness of the barriers in containing fire spread can be clearly seen by the burning locations on the ACM panels and PIR insulation. Generally, the absence of horizontal barriers (BI2, Fig 17b and Fig 18b) or non-activation of intumescent (BI3, Fig 17c and Fig 18c), results in a larger area of damage to the cladding system due to further vertical fire spread. The lack of vertical barriers (BI4, see Fig. 17d and Fig. 18d) results in a greater lateral fire spread within a cladding system.

With fully installed barriers (BI1, Fig 17a and Fig 18a), the burning locations on the ACM panels are mainly restricted on the panel just above the chamber (Fig. 17a) with the white/light-grey area representing the burnt off ACM locations, while the red dots represent locations of burning ACM. The burning locations on the ACM in the upper panels are only at the edges of these panels. The ignition of PIR (Fig 18a) is caused by exposing the PIR to the external fire after the protecting ACM panel has been burnt off. As a result, the burning locations on the PIR are only limited to the area just above the chamber (Fig. 18a).

With the removal of three horizontal barrier rows on the main wall in scenario BI2, the burning locations spread to most of the area of the ACM panels on the main wall (Fig. 17b). The burnt off ACM extends to the top of the test facility along the vertical edge of the panels on the main wall near the corner. Due to the lack of some horizontal barriers, the burning of PIR spreads to most of the main wall (Fig. 18b). With the inactive intumescent on three horizontal barrier rows on the main wall in scenario BI3, the burning locations spread to most parts of the ACM panels on the main wall (Fig. 17c). The burnt off ACM region extends to the middle panel on the main

wall. Due to the inactive state of the intumescent and the burnt off portions of the ACM panels, the burning of PIR occurs in the bottom and the middle panel on the main wall (Fig. 18c).

With the removal of part of a vertical barrier in Scenario BI4, the burning ACM locations are similar to that in the scenario with fully installed barriers on the main wall; the burnt off ACM is limited in the bottom panel on the main wall. However, without this part of vertical barrier, the fire has already spread to the wing wall via the middle section of the main wall (Fig. 17d). The burning of PIR has also laterally spread over onto the wing wall (Fig. 18d).

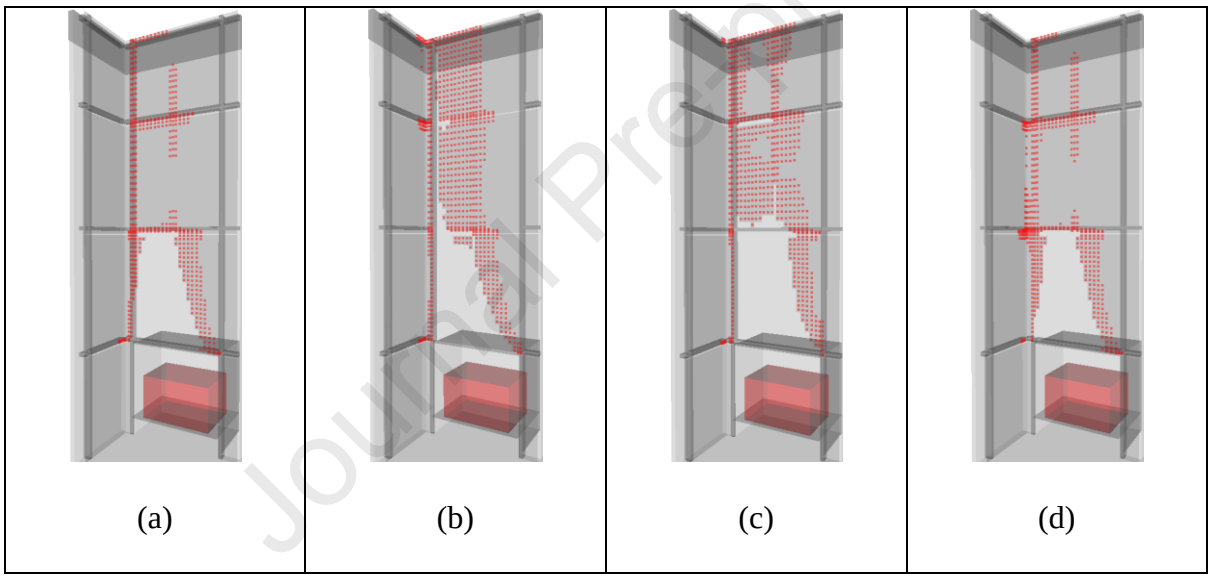


Fig. 17. Burning ACM panel locations (red dots) and burnt off ACM (light grey area) at 490s in barrier scenario (a) BI1 with full barriers; (b) BI2 with the lack of three horizontal barrier rows; (c) BI3 with inactive intumescent at three horizontal barrier row and (d) BI4 with the lack of part of a vertical barrier.

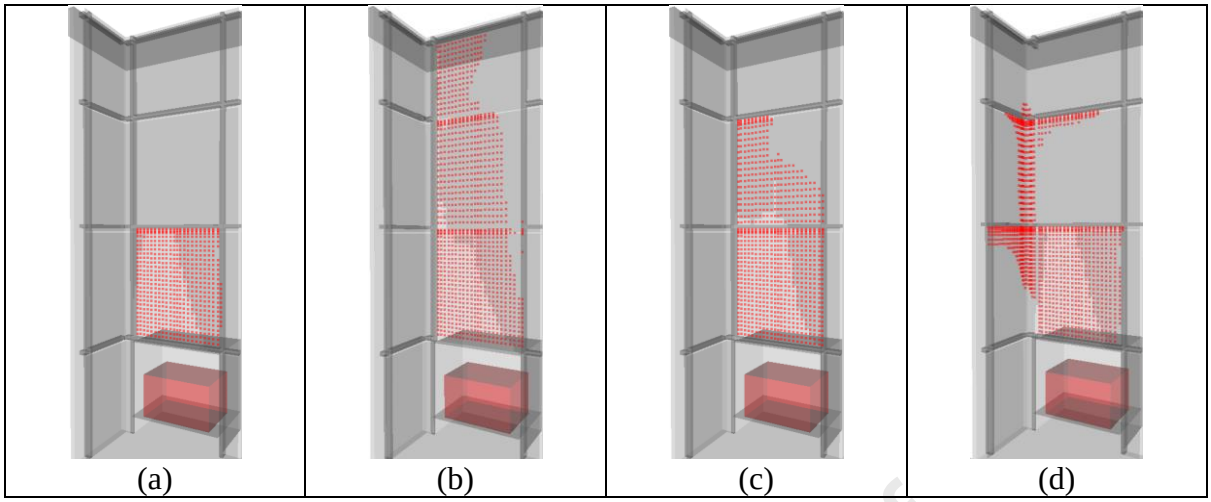


Fig. 18. Burning PIR insulation locations (red dots) at 490 s in barrier scenarios (a) BI1 with full barriers; (b) BI2 with the lack of three horizontal barrier rows; (c) BI3 with inactive intumescent at three horizontal barrier row and (d) BI4 with the lack of part of a vertical barrier.

These simulations highlight the importance of correctly installing intumescent barriers and explain the impact on the Grenfell Tower fire of poorly installed or missing fire barriers on the vertical and lateral fire spread.

### 5.6 Impact of the top window pod

In the DCLG BS 8414 tests, aluminium pods were installed on the top and at the two sides of the combustion chamber [14]. The window pod extends approximately 0.03 m beyond the front face of the finished cladding system. The lowest horizontal barrier is just above the top window pod. The top window pod is still intact after the termination of the fire in DCLG BS 8414 test 1. Therefore, the cavity of the cladding system is actually protected by the top window pod and its adjacent horizontal barrier. The impact of the window pod on fire development is investigated by a simulation scenario which is the same as DCLG test 1 but with the top aluminium pod removed (see Supplementary Material Section S7). With the removal of the aluminium window pod, the failure occurs after 300 s i.e., 60 s sooner. Interestingly, in the Grenfell Tower cladding system, there was no such window pod beneath the cladding. It is

unclear why these aluminium barriers were included in the DCLG tests as they clearly provide additional protection to the cavity and the ACM panels.

### 5.7 Impact of cavity thermocouple location

In the DCLG BS 8414 tests, the thermocouples used to record the cavity temperatures are located 7.0 m above the floor, which is just above the horizontal barrier between the upper two ACM panels. It is interesting to investigate if the pass/fail status of a cladding system is sensitive to the precise location of the cavity thermocouples. Presented in Fig. 19 is the predicted temperature profile along a vertical line passing through the middle cavity thermocouple in DCLG test 5 at 1240 s. It is noted that the cladding system in this specific test case passes the BS 8414 test in both the DCLG experimental study and the corresponding CFD simulation presented in this study (See Table 5).

The predicted temperature at the middle thermocouple after 1240 s, is 195 $^{O}$C, far below the critical temperature rise of 600 $^{O}$C required to trigger a fail according to Criterion 2. However, at a location just beneath the horizontal barrier (some 0.3 m below the reported thermocouple location), the predicted temperature is 642 $^{O}$C. While this temperature is high enough to change the status of the cladding system from a pass to a fail, it occurs after 1240 s, well past the 15 minutes (900 s) critical time specified in Criterion 2. Nevertheless, this demonstrates that selectively locating a thermocouple by a few centimetres within the cavity could significantly increase or decrease the recorded temperatures and could possibly influence the outcome of the test.

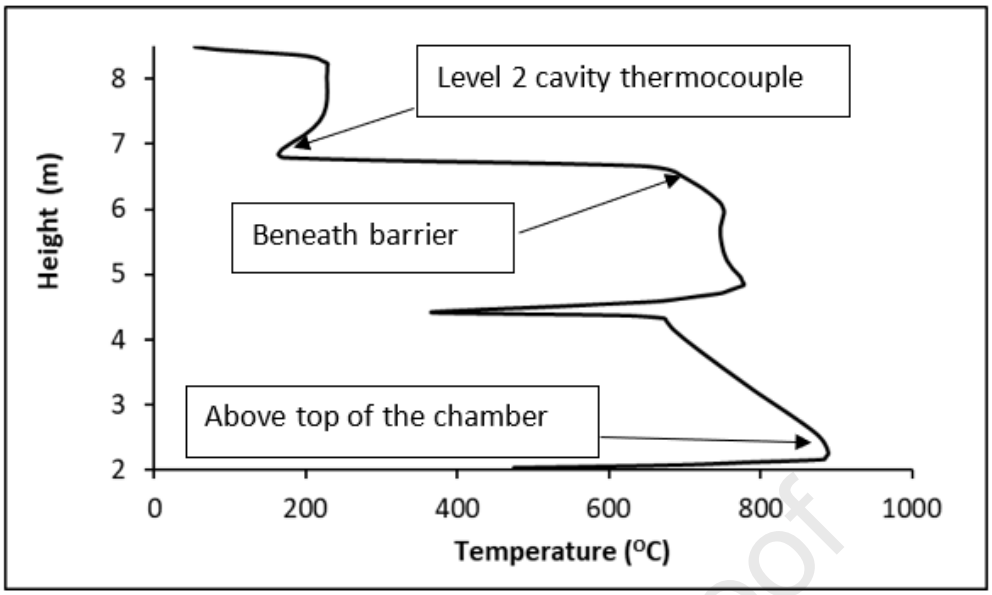


Fig. 19. Predicted temperatures along vertical line passing the middle cavity thermal couple at 1240 s in DCLG test 5.

## 6. Study Limitations

Fire propagation over a cladding system involving ACM panels is a complex process. The ignition of an ACM panel in which the burnable core material is protected by aluminium sheets is in and of itself very complex. Given the computational costs associated with running CFD fire simulation models, it is not practical to include the detailed complex processes of ACM burning in simulations of large-scale fires involving ACM cladding. It is thus necessary to introduce modelling simplifications that reduces the computational burden, while hopefully not compromising the validity of model predictions. Furthermore, not all thermal properties for the materials used in the testing are readily available or known. In addition, some material properties (such as those for fire retarded materials) may be strongly temperature dependent [57], further complicating their specification in models. It is thus necessary to approximate these values and so it is essential to understand the impact these uncertainties may have on the numerical predictions. Some of the limitations associated with these simplifications are identified below.

- Within the model the surface ignition temperature for an ACM panel with PE core is assumed to be 550 $^{O}$C and a value of 480 $^{O}$C is assumed for its unprotected edges (these temperatures are between the surface ignition temperature of the burnable ACM core material and the melting point of aluminium);
    - The modelling approach would benefit from additional experimental data characterising the ignition conditions of cladding materials, both for ACM and for the insulation, which is also covered with a thin layer of aluminium foil;
- Within the model, a simple approach to the activation of intumescent has been adopted. The activation of intumescent is a gradual process but is simply modelled as a temperature dependent switch, with a critical activation temperature adopted from previous modelling literature [30]. Furthermore, it is assumed to immediately fully activate when the critical temperature is reached i.e., without a time delay;
    - The modelling approach would benefit from experimental data on the performance (activation time and activation conditions) of the cavity barriers;
- The HRR curve for the wood crib fires used in each of the DCLG BS 8414 trials is unknown. Thus, the simulations presented in this work are based on an HRR curve derived from a measured curve for a BS 8414 test without installed cladding with a peak HRR of 2.5 MW. Furthermore, the same wood crib HRR is used for all the BS 8414 DCLG tests, when in reality, the HRR is likely to have been different in each test.
    - When the model is used to investigate an arbitrary BS 8414 test, it should be kept in mind that the HRR curve of the actual wood crib fire can be different from the HRR curve adopted in this study;

- The complexity of the wood crib fire behaviour. The burning of wood cribs is complicated; the wood crib fire model is calibrated for the standard BS 8414 test with the standard wood crib size (1.5 m long, 1.0 m wide and 1.0 m high) by comparing the simulation results with the observed flame shape and the measured temperatures of a particular BS 8414 test.
    - The wood crib fire model should be re-validated if the volume/size and structure of the wood crib changes.

- The properties of FR PE are strongly temperature dependent, especially during the endothermic decomposition process of the retardant components [57]. In this study, the endothermic decomposition process is omitted, and the thermal properties are assumed to be that for PE but with a relatively large specific heat value, which is derived by comparing the experimentally observed ignition times of ACM with PE and FR PE cores.
- Some of the required thermal properties of the tested materials are unknown, for example, conductivity and specific heat of FR PE and the conductivity of Phenolic. As a result, some material properties in the simulations are found from literature sources, which might not be the same as those used in the DCLG BS 8414 tests [14] while some were roughly estimated based on similar materials. Selective sensitivity studies were performed to assess the reliability of model predictions to these parameter values (see Supplementary Material Section S8). For example, the density of FR PE used in DCLG test 3 simulation i.e., 925 kg/m$^3$ was increased to 1265 kg/m$^3$, a change of 37%. It is noted that this test failed due to the external flame exceeding the height of the rig. The time for the rise of the level 2 temperature to exceed 600 $^{O}$C was delayed by 19.7% and thus did not change the conclusions of the simulation. Furthermore, the predicted time for this cladding system to fail is delayed by 9.9% and so the test is predicted to fail at

approximately the same time, and so does not change the conclusions of the simulations. In addition, the conductivity of phenolic used in the DCLG test 7 simulations i.e., 0.02 W/mK was increased to 0.03 W/mK, a change of 50%. This resulted in a delay of 1.5% in the time for the rise of the level 2 temperature to exceed 600 $^{O}$C and did not change the conclusions of the simulation. However, this test failed due to the external flame exceeding the height of the rig. The time for this failure is delayed by 1.5% and so the test is predicted to fail at approximately the same time, so does not change the conclusions of the simulations. Thus, while it is preferable to use the correct values for the material properties, if available; using reasonable approximations to material properties based on those for similar materials, with appropriate sensitivity analysis, is likely to produce acceptable results.

- The dripping behaviour resulting from the burning of plastics has not been modelled in this study. The lack of this feature may significantly affect the reliability of the model if the model is used to simulate high-rise building cladding fires. However, this limitation is unlikely to significantly affect the application of the model to BS 8414 tests because much of the fuel lost due to dripping is likely to contribute to the fire plume generated by the wood crib and so be accounted for in the test fire.
- The falling of debris (parts of cladding panels) has not been considered in the model. For the BS 8414 tests [14], large parts of cladding panels were not observed to break lose and fall to the ground. However, it is possible for large pieces of cladding panels to randomly break off either due to fire damage or incorrect panel installation. If parts of the ACM panel above the fire break off, this could possibly slow the vertical and lateral fire spread (less fuel) or it may enhance fire spread by exposing the insulation directly to the external fire plume.

- In all of the simulations, it was assumed that all the internal cavity fire barriers and intumescent were correctly installed. If incorrectly installed or missing, this will enhance the fire spread as has been demonstrated. Likewise, it has been assumed that the DCLG experiments had the internal cavity barriers correctly installed, even though it is known that in the Grenfell Tower cladding wall installation, cavity barriers had not always been installed or installed correctly. It is unclear whether cavity barrier installation is checked during the set-up of the experimental tests.
- Calorimetry data used to define the combustion characteristics of the ACM panels and associated component materials assumed an irradiance level of 50 kW/m$^2$. While this value is typically used to simulate cladding wall fires [30-33] and enclosure spread fires [36-40, 43], it is possible that the ACM panels can be subjected to higher irradiance levels, especially in regions where the ACM is completely consumed by the fire resulting in burn through, and possibly when the wood crib fire has reached its peak development. Use of combustion data based on higher irradiance levels could speed up the burn through process and impact the speed of fire development, assuming that high radiative flux levels occur sufficiently early in the fire. Therefore, cone calorimeter data for ACM materials should be collected at higher irradiance levels and used in models to assess the sensitivity of the fire spread model.
- The presence of gaps around the edges of installed ACM panels in external cladding wall systems can have a significant impact on fire propagation and so must be carefully considered in actual installations, in experimental fire tests and in modelling. The modelling of the horizontal and vertical gaps in the model attempted to faithfully represent the gaps in the experimental setup however, simplifications in the treatment of the vertical gap were necessary given the

complexity and uncertainty in gap specification. Detailed experimental and modelling studies of gap configuration are required to better understand the sensitivity of fire propagation to gap geometry.

- As seen in Fig. 10, the cladding in DCLG test 6 sustained some of the least fire damage compared to the other six tests. In this test, the cladding was first ignited at approximately 500 s after the ignition of the wood crib [14]. The physical extent of the burning locations extends to approximately 3.8 m above the chamber at 1920 s. The average vertical flame spread rate in this test was approximately 0.0027 m/s. In comparison, given the greater fire damage observed in the other tests, the vertical flame spread rate for the other six tests would be larger than that observed in DCLG test 6. Therefore, the successful reproduction of all seven DCLG fire tests, even when using a much smaller flame spread rate (i.e., 0.0001 m/s), implies that the impact of ignition Criterion (b) is negligible in these simulations due to the more significant impact of the large wood crib fire, which allows the flame sheet to directly cover the cladding. However, when applying this model to large building fires, even with the same cladding materials, in which the fire spread is sustained by the heat released from the combustion of the cladding only, the use of a realistic spread rate in Criterion (b) may be necessary, especially for cladding systems with low HRR materials.

## 7. Conclusions

In the aftermath of the Grenfell Tower fire tragedy, there has been renewed interest in assessing the fire performance of high-rise building cladding systems. The BS 8414 test is currently considered an appropriate large-scale test suitable for assessing cladding systems however, given the high costs associated with BS 8414 testing and relatively few facilities capable of undertaking such testing it is important to develop appropriate means to reduce these costs.

This study has developed a BS 8414 model to numerically simulate the large-scale BS 8414 cladding fire test using the SMARTFIRE simulation software. Furthermore, the modelling of the BS 8414 test has highlighted areas where the modelling could be used to provide additional insight into how cladding systems perform in a BS 8414 scenario to support and extend the current testing protocol.

The BS 8414 model has been validated using data from the seven DCLG BS 8414 tests and has been shown to be able to correctly predict pass/fail results and mechanisms leading to failures. The model was also capable of reproducing flame size and shape as part of the pass/fail process, external and cavity temperatures at Level 2 in good agreement with experimental results, and the locations of burnt/burning cladding components.

The BS 8414 Simulator has a range of capabilities, including predicting burning rates of individual components of the cladding system, predicting temperature profiles at any arbitrary location, activation state of barrier intumescent as a function of time and predicting burning locations of the ACM panel and insulation.

In addition to reproducing the BS 8414 test, the BS 8414 model can be used to investigate factors affecting fire spread in cladding systems. Presented in this paper are several insights on cladding design that impacts fire spread. For example, the analysis demonstrates that cavity size can significantly impact lateral and vertical fire spread rates on the ACM panels, with the larger the cavity the faster the lateral and vertical spread. For ACM with a PE core, reducing the mass of PE in the panels impacts the speed of vertical fire spread predicted in the BS 8414 simulations, with a 30% reduction in the mass of PE (for example by dripping) delaying the time to failure by 60 s. Furthermore, it was demonstrated that natural variation in the peak

HRR of wood cribs (reported to be between 2.5 MW and 3.5 MW) could make the difference between a pass or fail in the BS 8414 test. This observation brings into question the repeatability of the BS 8414 test and hence its suitability as a standard. It is suggested that the wood crib in the BS 8414 test be replaced by a gas burner which would improve the repeatability of the test. Another issue in the BS 8414 tests conducted for DCLG, a metal window pod was used to provide extra protection to the cavity in the cladding system. This window pod is not applied in practical building wall cladding systems. Based on the predicted cavity temperatures, the use of a window pod is likely to delay the failure of a wall cladding system, that uses PE as the ACM core and PIR as the insulation, by approximately 60 seconds. In addition, the precise location of thermocouples within the BS 8414 test can significantly impact the assessment of cladding performance. Thus, great care must be taken in the precise location of thermocouples.

One important finding from this study is that an Aluminium-based ACM surface ignition temperature of 550 $^{O}$C is applicable for all seven DCLG BS 8414 tests with various core materials where the ignition temperature of the core is less than 550 $^{O}$C. .

Like any model, the presented BS 8414 model is not without its limitations. While the thermal properties are critical model parameters for cladding fire simulations, the specific heat for some common building materials are unavailable from the open literature, such as FR PE, phenolic foam etc. . Clearly, the model would benefit from a more extensive set of BS 8414 data sets to further validate the Aluminium-based ACM surface ignition temperature and edge ignition temperature concept recommended in this study. Furthermore, in the presented model, the wood crib fire was described by a HRR model based on a BS 8414 test without cladding. When

attempting to reproduce an actual BS 8414 test, it is possible that the wood crib fire could be significantly different due to natural variations in how wood cribs burn.

The current BS 8414 model could potentially be applied to simulate cladding fires for high rise buildings if the dripping feature in the burning of plastic material is appropriately addressed. The technical computation of fuel re-location could be accommodated in the CFD modelling if appropriate characterisation of the dripping losses and dripped fuel arrival locations can be determined from incidents or experimental studies. Dripping fuel losses that contribute to the flame sheet, whilst dropping, are beyond the capabilities of the current modelling approaches. Work on the BS 8414 model continues with an extension to consider living or green walls. In addition, the BS 8414 model is being used to explore mitigation strategies to prevent rapid vertical and lateral fire in high-rise buildings clad with combustible cladding systems.

To the authors' best knowledge, the cladding fire simulations presented in this study are amongst the first to include ACM panels with a FR PE core. The challenge in these simulations is the representation of the complicated FR PE behaviour in fires, especially during the endothermic decomposition process of the retardant component. The successful reproduction of three BS 8414 tests (DCLG test 3, DCLG test 4, DCLG test 7) provides some justification of the appropriateness of the assumed parameter values for FR PE used in this study. In further studies, temperature dependent thermal properties including a simple endothermic decomposition model will be applied to improve the model reliability for FR PE cladding fire simulations.

**Acknowledgements**
This research was supported and part funded by the University of Greenwich Innovation fund 2022 (14648) and 2023 (1-R1110-321D-P13436). The authors gratefully acknowledge the contribution from three anonymous reviewers who made valuable contributions to improve the clarity and quality of this work.

**References**

[1] Peng L., Ni Z., Huang X., Review on the fire safety of exterior wall claddings in high-rise buildings in China, Procedia Engineering, Vol. 62, pp. 663-670, 2013. https://doi.org/10.1016/j.proeng.2013.08.112

[2] Chen T., Yuen A., Yeoh G., et al., Fire Risk Assessment of Combustible Exterior Cladding Using a Collective Numerical Database, Fire, Vol. 2, 2019. http://dx.doi.org/10.3390/fire2010011

[3] Moore-Bick M., Grenfell tower inquiry: phase 1 report, report of the public inquiry into the fire at grenfell tower on 14 june 2017, ISBN 978-1-5286-1602-7, 2019.

[4] Approved Document B: Fire safety- Volume 2, Buildings other than Dwellinghouses, London ISBN 978 1 914124 03 7, 2020, p. 204. https://assets.publishing.service.gov.uk/government/uploads/system/uploads/attachment_data/file/937932/ADB_Vol2_Buildings_other_than_dwellings_2019_edition_inc_2020_amendments.pdf

[5] Amendments to the Approved Documents, June 2022. https://www.gov.uk/government/publications/fire-safety-approved-document-b. Last accessed on 21 July 2022.

[6] BS EN 13501-1:2018, Fire classification of construction products and building elements, BSI Standards Limited, London, 2019.

[7] BS 8414-1:2015+A1:2017. Fire performance of external cladding systems – Part 1: Test method for non-loadbearing external cladding systems applied to the masonry face of a building. British Standards Institution. London, 2017.

[8] Colwell S., Baker T., Fire performance of external thermal insulation for walls of multistorey buildings, 3rd version, Watford: IHS BRE Press, UK, 2013.

[9] Schulz J., Kent D., Crimi T.A.C., Glockling J.L.D. and Hull T.R., A Critical Appraisal of the UK's Regulatory Regime for Combustible Facades, Fire Technology, Vl. 57, pp. 261-290, 2021. https://doi.org/10.1007/s10694-020-00993-z

[10] BS 8414-1, Fire performance of external cladding systems – Part 1: Test method for non-loadbearing external cladding, BSI Standards Limited, 2020.

[11] Moore-Bick M., Grenfell tower inquiry: phase 2 report, Volume 7. report of the public inquiry into the fire at grenfell tower on 14 june 2017, ISBN 978-1-5286-5080-9, 2024.

[12] Guillaume E., Fateh T., Schillinger R., et al., Study of fire behaviour of facade mock-ups equipped with aluminium composite material-based claddings, using intermediate-scale test method, *Fire and Materials,* Vol. 42, pp. 561-577, 2018. https://doi.org/10.1002/fam.2635

[13] Agarwal G., Wang Y., Dorofeev S., Fire performance evaluation of cladding wall assemblies using the 16-ft high parallel panel test method of ANSI/FM 4880, *Fire and Materials,* Vol. 45, pp. 609-623, 2021. https://doi.org/10.1002/fam.2852

[14] BRE Global Client reports , report number B137611-1037 (DCLG test 1; DCLG test 2; DCLG test 3; DCLG test 4; DCLG test 5; DCLG test 6; DCLG test 7), BRE Global, UK, 2017.

[15] Bjegović D., Pečur I., Milovanović B, Rukavina M., Comparative full-scale fire performance testing of ETICS systems, *Građevinar,* Vol. 68, pp. 357-369, 2016. https://doi.org/10.14256/JCE.1347.2015

[16] Report detailing the testing of an HPL rainscreen cladding system tested in accordance with the requirement as described in British Standard 8414, Report Number FPA-101856.002, The Fire Protection Association, London, UK, 2019.

[17] Zhou, R, Yu, Z, Chen, Z, Qian, J, Jiang, J. Fire test of metal sandwich plates during a window spill fire. *Fire and Materials*. 2022; 46(8): 1180-1196. doi:10.1002/fam.3061

[18] Čolić, A., Pečur, I.B. Influence of Horizontal and Vertical Barriers on Fire Development for Ventilated Façades. *Fire Technol* **56**, 1725–1754, 2020. https://doi.org/10.1007/s10694-020-00950-w

[19] McGrattan K., Hostikka S., Mcdermott R., Floyd J., Weinschenk C., Overholt K. Fire Dynamics Simulator (FDS Version 6.0.1) Technical Reference Guide, Vol. 1 Mathematical model. Gaithersburg, Maryland, United States: National Institute of Standards and Technology; 2013.

[20] Ding Y, Wang C, Lu S. Modeling the pyrolysis of wet wood using FireFOAM. Energy Conver Manag. 2015;98:500-506. https://doi. org/10.1016/j.enconman.2015.03.106.

[21] Ewer J., Jia F., Grandison A., Galea E.R. and Patel M.K., "SMARTFIRE V4.4 User Guide and Technical Manual, Fire Safety Engineering Group, University of Greenwich, UK, 2017.

[22] Yuen A.C.Y, Chen T.B.Y., Li A., et al., Evaluating the fire risk associated with cladding panels: An overview of fire incidents, policies, and future perspective in fire standards, Fire and Materials. 2021; 45: 663–689. https://doi.org/10.1002/fam.2973

[23] Miao L, Chow C, A study on window plume from a room fire to the cavity of a double-skin façade, Applied Thermal Engineering, Volume 129, 2018, Pages 230-241. https://doi.org/10.1016/j.applthermaleng.2017.09.125.

[24] Livkiss K, Husted B, Beji T, Hees P, Numerical study of a fire-driven flow in a narrow cavity, Fire Safety Journal, Volume 108, 2019, 102834. https://doi.org/10.1016/j.firesaf.2019.102834.

[25] Hajduković, M., Knez, N., Knez, F. *et al.* Fire Performance of external thermal insulation composite system (ETICS) facades with expanded polystyrene (EPS) insulation

and thin rendering, Fire technology, Volume 53, 173-209, 2017. https://doi.org/10.1007/s10694-016-0622-2

[26] Anderson, J, Boström, L, Jansson McNamee, R, Milovanović, B. Modeling of fire exposure in facade fire testing. *Fire and Materials*. 2018; 42: 475–483. https://doi.org/10.1002/fam.2485

[27] Kotzen B., Galea E.R., Mosco S., Wang Z., Ewer J., Jia F., Fire safety risks of external living walls and implications for regulatory guidance in England, Fire Safety Journal, Volume 139, 2023, https://doi.org/10.1016/j.firesaf.2023.103816.

[28] Hassan M.K., Hossain M.D., Gilvonio M., Rahnamayiezekavat P., Douglas G., Pathirana S., Saha S., Numerical investigations on the influencing factors of rapid fire spread of flammable cladding in a high-rise building. Fire. 2022; 5(5):149. https://doi.org/10.3390/fire5050149

[29] Dréan V., Girardin B., Guillaume E., Fateh T., Numerical simulation of the fire behaviour of façade equipped with aluminium composite material-based claddings—Model validation at intermediate scale, *Fire and Materials,* Vol. 43, pp. 839-856, 2019. https://doi.org/10.1002/fam.2745

[30] Dréan V., Girardin B., Guillaume E., Fateh T., Numerical simulation of the fire behaviour of facade equipped with aluminium composite material-based claddings-Model validation at large scale, Fire and Materials, Vol. 43, pp. 981-1002, 2019. https://doi.org/10.1002/fam.2759

[31] Dréan, V., Girardin, B., Chiva, R., Guillaume, É., and Fateh, T,. Numerical Investigation of the Thermal Exposure of Façade During BS 8414 Test Series: Influence of Wind and Fire Source. Fire Technology, 2023:59, 217-246. https://doi.org/10.1007/s10694-022-01274-7

[32] Guillaume E., Dréan V., Girardin B. et al., "Reconstruction of Grenfell Tower fire. Part 3—Numerical simulation of the Grenfell Tower disaster: Contribution to the understanding of the fire propagation and behaviour during the vertical fire spread," *Fire and Material,* vol. 33, pp. 35-57, 2020. https://doi.org/10.1002/fam.2763

[33] Guillaume, E, Dréan, V, Girardin, B, Fateh, T. Reconstruction of the Grenfell Tower fire – Part 4: Contribution to the understanding of fire propagation and behaviour during horizontal fire spread. *Fire and Materials*. 2020; 44: 1072–1098. https://doi.org/10.1002/fam.2911

[34] Jia F., Patel M.K., Galea E.R., Grandison A. and Ewer J., CFD Fire Simulation of the Swissair Flight 111 In-flight Fire – Part II: Fire Spread within the Simulated Area, The Aeronautical Journal of the Royal Aeronautical Society, Vol. 11, pp. 303-331, 2006. https://doi.org/10.1017/S0001924000013178

[35] Hu X., Wang, Z., Jia, F., Galea E.R., Numerical investigation of fires in small rail car compartments, Journal of Fire Protection Engineering, Vol. 22, pp. 245-270, 2013. https://doi.org/10.1177%2F1042391512459640

[36] Galea E.R., Wang Z., Veeraswamy A., Jia F., Lawrence P. J. and Ewer J., Coupled fire/evacuation analysis of station nightclub fire, in *Proc of 9th IAFSS Symp, Sep. 21-26*, Karlsruhe, Germany, pp 465-476, 2008.

[37] Galea, E.R., Filippidis, L., Wang, Z., Ewer, J, Fire and evacuation analysis in BWB aircraft configurations: computer simulations and large-scale evacuation experiment, *The Aeronautical Journal of the Royal Aeronautical Society*, Vol. 114, pp. 271-277, 2010. https://doi.org/10.1017/S0001924000003717

[38] Galea E.R., Wang Z., Jia F., Numerical investigation of the fatal 1985 Manchester Airport B737 fire, The Aeronautical Journal, Vol. 121, pp. 287-319, 2017. https://doi.org/10.1017/aer.2016.122

[39] Galea, E.R., Wang, Z., and Jia, F., Lawrence, P.J. and Ewer. J. , Fire safety assessment of Open Wide Gangway underground trains in tunnels using coupled fire and evacuation simulation, *Fire and Materials,* Vol. 41, pp. 716-737. https://doi.org/10.1002/fam.2413

[40] Wang Z, Jia F, Galea ER, Choi J.H., A forensic analysis of a fatal fire in an indoor shooting range using coupled fire and evacuation modelling tools, Fire Safety Journal, Vol. 91, pp. 892-900, 2017. https://doi.org/10.1016/j.firesaf.2017.03.029

[41] Magnussen B.F. and Hjertager B.H., "On mathematical modelling of turbulent combustion with special embassies on soot formation and combustion," 16th Symp. (Int.) on Combustion, the Combustion Institute, 1977.

[42] Barlow, R. S., Karpetis, A. N., Frank, J. H., and Chen, J.Y., "Scalar profiles and NO formation in laminar opposed-flow partially premixed methane/air flames", Combustion and Flame, Vol. 127, pp. 2102-2118, 2001. https://doi.org/10.1016/S0010-2180(01)00313-3

[43] Wang, Z., Jia, F., Galea, E.R., Ewer J. , Computational fluid dynamics simulation of a post-crash aircraft fire test, Journal of Aircraft, Vol. 50, pp. 164-175, 2013. https://doi.org/10.2514/1.C031845

[44] Private Communication, email from Prof Richard Hull, University of Central Lancashire, UK, 18 July 2019.

[45] McKenna S.T., Jones N., Peck G, et al., Fire behaviour of modern façade materials – Understanding the Grenfell Tower fire, Journal of Hazardous Materials, Vol. 368, No. 15, pp. 115-123, 2019. https://doi.org/10.1016/j.jhazmat.2018.12.077

[46] M. J. Hurley, *SFPE handbook of fire protection engineering, fifth edition*, Springer-Verlag New York, 2016.

[47] Thermal Properties of Plastic Materials. https://www.professionalplastics.com/professionalplastics/ThermalPropertiesofPlasticMaterials.pdf (accessed on the 24th, March 2023)

[48] Salem E., Khozemy E., Ali A., Potential flame retardancy of high-density polyethylene (HDPE) composite for possible use as a radiation shield, Progress in Nuclear Energy, Volume 165, 2023. https://doi.org/10.1016/j.pnucene.2023.104900.

[49] Stec A., Hull R., Assessment of the fire toxicity of building insulation materials, *Energy and Buildings,* Vol. 43, pp. 498-506, 2011. https://doi.org/10.1016/j.enbuild.2010.10.015

[50] Iffa, E., Tariku, F., Simpson, W.Y., Highly insulated wall systems with exterior insulation of polyisocyanurate under different facer materials: material characterization and long-term hygrothermal performance assessment. Materials 2020, 13, 3373. https://doi.org/10.3390/ma13153373

[51] Tseng C., Kuo K., Thermal properties of phenolic foam insulation, Journal of the Chinese Institute of Engineers, Vol. 25, No. 6, pp. 753-758 (2002).

[52] Faggiano B., Matteis G., Landolfo R., Mazzolani F., Behaviour of aluminium alloys structure under fire, *Civil Engineering and management,* Vol. 10, pp. 183-190, 2004. https://doi.org/10.1080/13923table730.2004.9636305

[53] Hossain M., Saha S., Hassan M., et al., Testing of aluminium composite panels in a cone calorimeter: A new specimen preparation method, Polymer Testing, Volume 106, 2022. https://doi.org/10.1016/j.polymertesting.2021.107454.

[54] Manzi-Nshuti C., Hossenlopp J., Wilkie C., Comparative Study on the Flammability of Polyethylene Modified with Commercial Fire Retardants and a Zinc Aluminum Oleate Layered Double Hydroxide, *Polymer Degradation and Stability,* Vol. 94, pp. 782-788, 2009. https://doi.org/10.1016/J.POLYMDEGRADSTAB.2009.02.004

[55] Hjohlman M., Försth M., Axelsson J., Design fire for a train compartment, SP Report 2009:08; Fire Technology, SP Technical Research Institute of Sweden, 2009.

[56] Heskestad, G., Flame Heights of Fuel Arrays with Combustion in Depth, pp. 427-438 in Fire Safety Science--Proc. Fifth Intl. Symp., Intl. Assn. for Fire Safety Science (1997).

[57] Hull T., Witkowski A., Hollingbery L., Fire retardant action of mineral fillers, Polymer Degradation and Stability, Volume 96, 2011, pp. 1462-1469. https://doi.org/10.1016/j.polymdegradstab.2011.05.006.

# CFD simulation of the BS 8414 test for Cladding Applications

Zhaozhi Wang, Fuchen Jia, Edwin R Galea*, John Ewer,

*Corresponding Author: e.r.galea@gre.ac.uk

***Centre for Safety, Resilience and Protective Security, Fire Safety Engineering Group,***

***University of Greenwich, Old Royal Naval College,***

***30 Park Row, Greenwich, LONDON SE10 9LS, UK***



Highlights:

- A CFD fire model capable of simulating BS 8414 test has been developed
- The model is validated using data from BS 8414 tests of seven cladding systems
- Cladding cavity size is predicted to significantly impact fire spread
- Natural variations in wood crib HRR can compromise validity of BS 8414 results
- 30% mass reduction of PE core delays failure of BS 8414 test by only 60s

**Declaration of interests**

☒ The authors declare that they have no known competing financial interests or personal relationships that could have appeared to influence the work reported in this paper.

☐ The authors declare the following financial interests/personal relationships which may be considered as potential competing interests: